energy&fuels

Review

Cite This: Energy Fuels 2018, 32, 7245−7261

pubs.acs.org/EF

Kinetic and Reactor Modeling of Catalytic Hydrotreatment of Vegetable Oils

Alexis Tirado,[†] Jorge Ancheyta,[*,‡] and Fernando Trejo[†]

[†]Instituto Politécnico Nacional, Centro de Investigación en Ciencia Aplicada y Tecnología Avanzada Unidad Legaria. Legaria 694, Col. Irrigación, Mexico City 11500, Mexico

[‡]Instituto Mexicano del Petróleo, Eje Central Lázaro Cárdenas Norte 152, San Bartolo Atepehuacan, Mexico City 07730, Mexico

ABSTRACT: Because of the growing world energy demand, biofuels obtained from the hydrotreatment of vegetable oils represent a renewable alternative to replace fossil fuels. The development of mathematical models is an accurate tool to design and simulate the performance of the reactor to predict product yields during the hydrotreatment of these oils. Better understanding of the different phenomena occurring during the hydrotreatment of vegetable oils and parameters influencing on this process by means of kinetic and reactor modeling is required. This was the motivation to develop an exhaustive review on different aspects of reaction kinetics, catalytic deactivation, and reactor modeling. Kinetics of model compounds and real feedstocks (oils) used to produce biofuels are analyzed and different assumptions for developing of reaction rate equations are discussed. It has been recognized that catalyst deactivation and reactor modeling must be deeply studied and supported with experimental data. There are few reported models that consider the mass transfer and temperature inside the catalytic particle. However, there are no models that consider the phase distribution and dispersion in the transient state, nor correlations to calculate the solubility of hydrogen in this type of system.

1. INTRODUCTION

The growing energy demand caused by increases in the population in the world around cities and industrial areas mainly, as well as international agreements to reduce the greenhouse gases caused by using fossil fuels, have motivated the study of new sources to produce renewable energy. One of the most promising environmentally friendly renewable alternatives is oil conversion to biofuels, because of the properties that they exhibit after being produced by catalytic transesterification, pyrolysis, and catalytic hydrotreating and the properties that are similar to those of fossil-based fuels.[1,2]

Before biofuels are synthesized, bio-oils must be obtained from crops or fats and further processed. Bio-oils are rich in oxygenated compounds such as free fatty acids, fatty acid esters, and triglycerides that have undesirable properties, such as low heating value, polarity, high viscosity, and corrosive effects. Biofuels are a promising alternative to fossil fuels, because of their sustainability in most of the cases and CO_2 neutral resources. When nonedible biomass is used as a source of bio-oils, then second-generation biofuels are obtained after treatment.[3,4] These fuels are considered renewable, because they can be produced from a large number of sources (oils/fats of vegetable or animals or even their waste), unlike fossil fuels that have finite reserves.

Biomass to produce liquid fuels could be produced via several processes. Three primary paths to obtain gas or liquid fuels are (1) gasification, (2) pyrolysis/liquefaction, and (3) hydrolysis. Syngas (CO and H_2) is obtained through gasification, which indeed is transformed to alkanes by Fischer−Tropsch synthesis; in methanol by methanol synthesis; or in hydrogen through water−gas shift reaction. Pyrolysis/liquefaction is used to obtain bio-oils. When hydrodeoxygenation is used, liquid fuels are obtained, or even hydrogen is synthesized by steam reforming from bio-oils. However, if triglycerides are fed, then catalytic hydrotreating (HDT) is able to transform them to liquid fuels. Bio-oils obtained by pyrolysis are processed through zeolites, and CO_2 and H_2O are released at atmospheric pressure and temperatures ranging from 300 °C to 600 °C, as reported elsewhere.[5] Other processes involve hydrodeoxygenation (HDO), as part of HDT as a major source of hydrocarbon fuels. Hydrogen that is required for HDO could be obtained from the water−gas shift reaction or steam reforming of bio-oils, using solar energy for example. In this case, hydrogen would not be obtained from steam methane reforming as usually produced. Hydrolysis from cellulosic biomass produce lignin-derived products that can be converted to gasoline. In addition, hydrolysis yields aqueous sugar to produce ethanol through fermentation or hydrocarbons by dehydration. A review including these conversion processes has been addressed vastly.[4]

Catalytic hydrotreating has been used for years to remove impurities (sulfur, nitrogen, metals, etc.) from fossil fuels through a series of chemical reactions, which are performed in a hydrogen-rich atmosphere over catalysts to increase the hydrogen-to-carbon ratio and remove these impurities in the form of H_2S or NH_3 mainly or by deposition of metals on catalysts. Since oxygen is commonly present in bio-oils or lignin-derived bio-oils, it is necessary to remove this atom to convert feedstocks to liquid fuels. Catalytic processes such as HDO is a common way to achieve this goal. Similarities among HDO in bio-oils and hydrodesulfurization (HDS) and hydrodenitrogenation (HDN) in petroleum occurs; however, in petroleum refining, the HDS and HDN reactions yield liquid

Received: March 20, 2018
Revised: May 29, 2018
Published: May 31, 2018

DOI: 10.1021/acs.energyfuels.8b00947
Energy Fuels 2018, 32, 7245−7261

Table 1. Summary of Conditions Used To Develop Kinetic Models Reported in Literature

feedstock	reactor type	reaction condition	catalyst[a]	conversion	ref
ethyl stearate	semibatch	270−360 °C, 17−40 bar, solvent (*n*-dodecane) atmosphere: Ar = 25 mL/min (5% H_2)	5Pd/C$^{(R)}$	41−100	16
stearic acid	semibatch	260−290 °C, 13−14.5 bar, solvent (*n*-dodecane) atmosphere: Ar = 25 mL/min (5% H_2), 6 h	Ni/γ-$Al_2O_3$$^{(O)}$	50−95	17
oleic acid	semibatch	320−380 °C, 20 bar (10% H_2), 1 h, 2000 rpm	FMoOx/Zeol$^{(R)}$	40−100	18
waste cooking oil	batch	300−375 °C, 1300 psi, 1000 rpm, 8 h 0.05% (w/w) catalyst/feed ratio	unsupported CoMoS$^{(S)}$	91−99	19
methyl heptanoate	batch	250−330 °C, 60−100 bar, solvent (*n*-hexadecane) 6 h, 700 rpm	Rh/ZrO_2 $^{(R)}$	15−90	20
methyl palmitic	batch	250−330 °C, 60−100 bar, solvent (*n*-hexadecane) 1 h, 700 rpm	Rh/$ZrO_2$$^{(R)}$		21
tripalmitin-tristearin	batch	280−360 °C, 30 bar, solvent (*n*-dodecane) 6 h, 1200 rpm	15NiAl$^{(R)}$	40−100	22
stearic acid TOFA	semibatch	300 °C, 7−30 bar, solvent (*n*-dodecane) 6 h, 1200 rpm	5Ni/γ-$Al_2O_3$$^{(R)}$, 5Ni/Y−H-80$^{(R)}$ 5Ni/$SiO_2$$^{(R)}$, Pd/C$^{(R)}$	99	25
FAME	semibatch	300 °C, 7−30 bar, solvent (*n*-dodecane) 6 h, 1200 rpm	5Ni/Y−H-80$^{(R)}$, Pd/C$^{(R)}$		26
rapeseed oil	fixed bed	300−380 °C, 10 bar, LHSV 2.7−9.8 h^{-1}	NiCu/CeO_2−$ZrO_2$$^{(R)}$	10−100	31
solvolytic primary oil	batch	300 °C, 80 bar, 1 h, 1000 rpm	NiMo/γ-$Al_2O_3$$^{(O\text{-}R\text{-}S)}$, Pd/C$^{(R)}$, $MoS_2$$^{(S)}$ NiMo/Al_2O_3−$SiO_2$$^{(R)}$, Pd/$\gamma$-$Al_2O_3$$^{(R)}$	43−94	27
solvolytic oils	batch	200−350 °C, 20−80 bar, solvent (tetralin) 1 h, 250−1000 rpm	NiMo/γ-$Al_2O_3$$^{(S)}$	83−85	28
jatropha oil	fixed bed	300−320 °C, 80 bar, LHSV = 2−12 h^{-1} catalyst amount = 2 g, H_2/HC = 1200−1500 l/l	CoMo/MTS$^{(S)}$	65−70	32
jatropha oil	fixed bed	320−360 °C, 80 bar, LHSV = 1−8 catalyst amount = 2.5 mL, H_2/HC = 1500	CoMo/$Al_2O_3$$^{(S)}$	89−98	33
jatropha oil	fixed bed	340−420 °C, 80 bar, WHSV = 0.5−12 catalyst amount = 2g, H_2/HC = 500−2500 Nl/l	NiW/SiO_2−$Al_2O_3$$^{(O)}$	29−100	35
palm oil	fixed bed	335−365 °C, 30−60 bar, τ = 15−45 min catalyst amount = 1.5 g	NiMo/γ-$Al_2O_3$$^{(S)}$	73−100	36

[a]State of catalyst: O = oxide form, R = reduce form, S = sulfide form.

hydrocarbons in single phases readily to be used as fuel. On the other hand, removing oxygen enhances water formation during HDO, which may deactivate the catalyst very fast during reaction by which bio-oils conversion into fuels is a processing challenge noticeably different from petroleum refining as reported.[6]

Once biofuels were produced by HDO, these liquid hydrocarbons have advantages compared with other products such as higher fuel efficiency with low losses in form of coke or gases, considering that their main products are *iso*- and *n*-alkanes free of aromatic and oxygenated compounds. As an example, when comparing with biodiesel conformed by fatty acids methyl esters, hydrotreated products are oxygen-free. In addition, green diesel obtained by HDO does not require consecutive improvement processes. These characteristics give similar physical and chemical properties to those of petrodiesel, such as cetane index and net heat value.[1,3,7]

Considering that the hydrotreating process of bio-oils is complex, because of the large number of physical and chemical phenomena occurring within the reactor, mathematical models are extensively used to predict reactor performance, determine optimal processing conditions, and carry out the scaling-up of reactors.

Since the production of biofuels through catalytic hydrotreating is a relatively new area of research and particularly considering the development of kinetic and reactor models, literature reports are scarce. That is the reason why, to date, no exhaustive reviews on the different kinetic and reactor models reported in the literature for the hydrotreatment of vegetable oil have been conducted. Recall that kinetic and reactor models that deal with the hydrotreatment of vegetable oils are scarce in the literature, and most of the reports are focused on experimentation with model compounds. The kinetics, catalysts, and reactor models for the hydrotreatment of vegetable oils and model molecules (e.g., triglycerides and fatty acids) are disclosed, as well as catalyst deactivation during the processing of oxygenated compounds.

2. KINETIC MODELS

2.1. Model Compounds. Experimental studies of the hydrotreatment of model compounds such as fatty acids (FA) and triglycerides (Tg) are typically performed to develop accurate and reliable reaction mechanisms, as well as evaluation of catalyst performance. In this way, when complex systems with several types of compounds such as bio-oils are hydrotreated, one can have an idea of reactions steps that are occurring in the reactor. Different studies focused on determining the reaction mechanisms occurring during hydrodeoxygenation (HDO) of bio-oil or model compounds[8−12] have improved the development of kinetic models.[13−15] Table 1 summarizes the operating conditions, feedstock, reactor, and catalyst types used in kinetic studies during the upgrading of bio-oils into green fuel. Snåre et al.[16] investigated the kinetic behavior of ethyl stearate over a commercial Pd/C catalyst in a semibatch reactor. A kinetic model was proposed in which ethyl stearate reacts to form its corresponding fatty acid to produce a paraffin.

DOI: 10.1021/acs.energyfuels.8b00947
Energy Fuels 2018, 32, 7245−7261

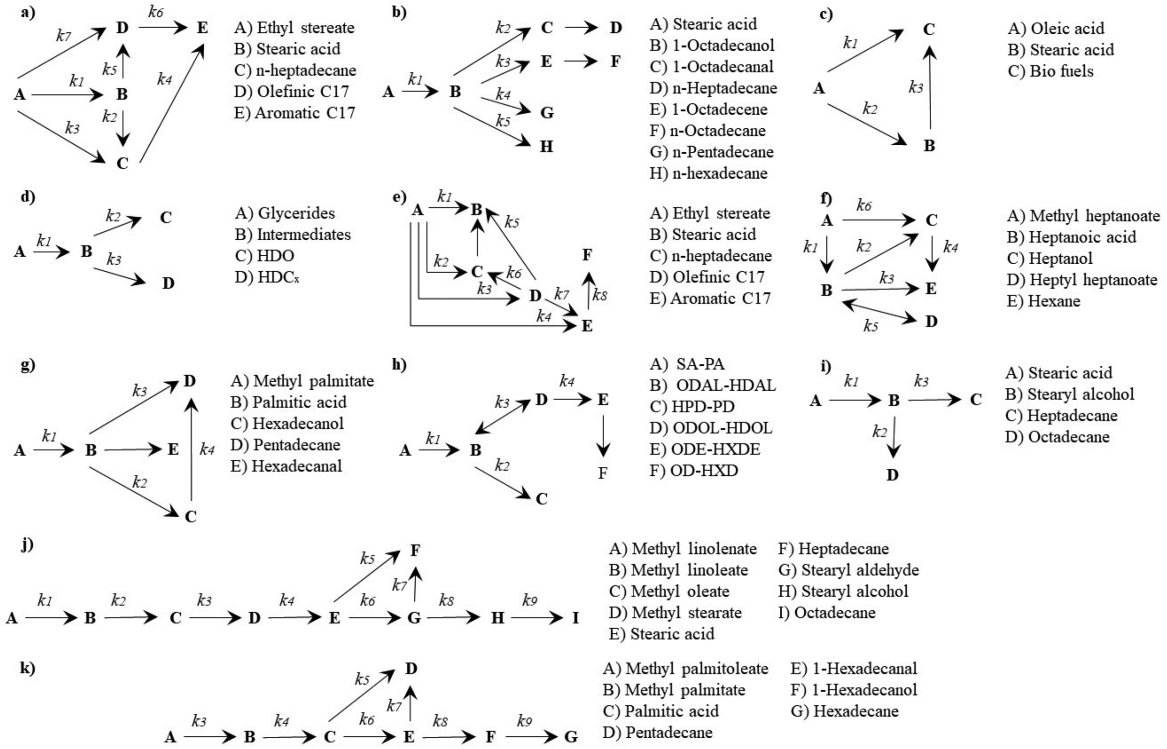

Figure 1. Reaction pathways for the hydrotreatment of model compounds.

However, dehydrogenation reactions can form olefins and even aromatic compounds, as shown in Figure 1a. Experimental concentration profiles of reactants and products were successfully fitted with the following Langmuir−Hinshelwood model:

$$r_j = \frac{k_j' C_i}{1 + K_A C_A + K_B C_B + K_C C_C + K_D C_D + K_E C_E} \quad (1)$$

where k_j' is an apparent reaction coefficient involving the reaction rate and equilibrium adsorption coefficients of reaction step j (j = 1, 2, 3, ...) and C_i is the concentration of reactant species i. The adsorption coefficients of product gases (i.e., CO_2, CO, ethylene, H_2) were neglected.

The reaction rate coefficients were determined at 300 °C and are summarized in Table 2. The results confirmed that the adsorption coefficients can be neglected; therefore, eq 1 takes the form of first-order power-law model. In subsequent experiments, it was shown that decarboxylation rate of stearic acid leads to an apparent reaction rate coefficient of 0.0065 mol L^{-1} min^{-1} and reaction order is close to zero. In addition, the higher the concentration of stearic acid, the faster the catalytic deactivation.

Kumar et al.[17] proposed a reaction mechanism focused on product distribution during HDO of stearic acid at several reaction times and temperatures with Ni/γ-Al_2O_3 as catalyst using a high-pressure batch reactor. The proposed model is shown in Figure 1b, where octadecanol is considered as an intermediate product, which undergoes dehydrogenation and decarbonylation reactions to finally produce heptane and 1 mol of CO. On the other hand, octadecanol is subjected to dehydration to form octadene, which becomes hydrogenated to octadecane. The formation of hexadecane and pentadecane is not completely clear and it was speculated to be final products of octadecanol. However, octadecanal was not detected during the HDO of stearic acid by which it was considered to be quickly converted to heptadecane. The reaction rates were expressed by power-law model assuming first reaction order because of hydrogen excess. The reaction rate of each step j is represented as follows:

$$r_j = k_j C_i \quad (2)$$

whereas the mass balance equation for each species is calculated by

$$\frac{dC_i}{dt} = \sum \nu_{ij} r_j \quad (3)$$

The estimated kinetic parameters are shown in Table 2. At all temperatures, k_2 is greater than other kinetic constants inferring a higher formation rate during conversion of alcohols to aldehydes. The reaction schemes depicted in Figures 1a and 1b show similar pathways, obtaining heptadecane as the main product. However, the selectivity of catalysts (Pd/C and Ni/γ-Al_2O_3, respectively) provides different product distribution and thus the values of some reaction rate coefficients are considerably different.

A similar model was used to determine the activity and product yields using a zeolite-based fluoride-ion functionalized molybdenum-oxalate catalyst (FMoOx/zeol) in the oleic acid (OA) HDO, as shown in Figure 1c.[18] The model takes into account the hydrogenation of the double bond in oleic acid to form stearic acid (SA) and finally the removal of oxygen atom. The reaction rate and mass balance equations were developed using the same assumptions made by Kumar et al.[17] to determine the kinetic parameters. Considering the value of k_1 as negligible, the values of k_2 and k_3 are shown in Table 2 where the hydrogenation rate of oleic acid (k_2) is much higher than the removal rate of O atoms in stearic acid (k_3).

Zhang et al.[19] proposed a kinetic model based on decomposition of waste cooking oil glycerides during HDO on

DOI: 10.1021/acs.energyfuels.8b00947
Energy Fuels 2018, 32, 7245−7261

Table 2. Kinetic Parameters Determined during the HDO of Model Molecules[a]

	Kinetic Parameters (s^{-1})								
	k_1	k_2	k_3	k_4	k_5	k_6	k_7	k_8	k_9
Pd/C, Model of Snåre et al.[16] (Figure 1a)									
temperature (°C)									
300	1.04×10^{-13}	2.18×10^{-5}	1.68×10^{-5}	2.42×10^{-14}	4.12×10^{-5}	3.85×10^{-6}	7.58×10^{-6}		
Ni/γ-Al_2O_3, Model of Kumar et al.[17] (Figure 1b)									
temperature (°C)									
260	4.20×10^{-5}	3.55×10^{-4}	8.44×10^{-6}	6.03×10^{-6}	1.30×10^{-5}				
270	6.43×10^{-5}	1.52×10^{-3}	2.43×10^{-5}	1.96×10^{-5}	4.57×10^{-5}				
280	1.59×10^{-4}	3.68×10^{-3}	6.70×10^{-5}	1.58×10^{-4}	3.34×10^{-4}				
290	3.24×10^{-4}	7.39×10^{-3}	7.59×10^{-5}	5.33×10^{-4}	1.03×10^{-3}				
E_a (kJ/mol)	175.4	250	190.9	387.7	377.2				
A_0	5.57×10^{12}	1.34×10^{21}	4.77×10^{13}	5.08×10^{32}	1.08×10^{32}				
FMoOx/Zeol, Model of Ayodele et al.[18] (Figure 1c)									
temperature (°C)									
320		0.150	0.038						
340		0.200	0.045						
360		0.280	0.052						
E_a (kJ/mol)		98.7	130.3						
A_0		2.85×10^{13}	3.95×10^{12}						
CoMoS, Model of Zhang et al.[19] (Figure 1d)									
temperature (°C)									
300	8.3×10^{-5}	7.36×10^{-6}	2×10^{-5}						
340	4.3×10^{-4}	2.87×10^{-5}	8×10^{-5}						
375	1.7×10^{-4}	5.9×10^{-5}	2×10^{-4}						
CoMoS, Model of Zhang et al.[19] (Figure 1e)									
temperature (°C)									
375	3.21×10^{-5}	1.39×10^{-4}	1.14×10^{-5}	5.94×10^{-5}	3.03×10^{-5}	1.06×10^{-5}	5.65×10^{-6}	3.5×10^{-4}	
15NiAl, Model of Yenumala et al.[22] (Figure 1h: Stearic Acid to *n*-Alkene)									
temperature (°C)									
280	6.5×10^{12}	4.17	1.5×10^{6}	1.5×10^{6}					
300	7.83×10^{12}	10	3×10^{6}	3.33×10^{6}					
320	15.8×10^{12}	16.67	5.83×10^{6}	14.7×10^{6}					
340	37.3×10^{12}	31.68	10×10^{6}	37.3×10^{6}					
360	46.7×10^{12}	52.5	15×10^{6}	85×10^{6}					
E_a (kJ/mol)	90.7	84.8	152.7	76					
A_0	1.67×10^{9}	1.61×10^{2}	3.62×10^{8}	0.88×10^{-4}					
15NiAl, Model of Yenumala et al.[22] (Figure 1h: Palmitic Acid to *n*-Alkene)									
temperature (°C)									
280	7.15×10^{12}	4.17	1.15×10^{6}	1.17×10^{5}					
300	8.17×10^{12}	9.17	3.0×10^{6}	1.67×10^{5}					
320	12×10^{12}	16.67	5.82×10^{6}	3.33×10^{5}					
340	37.3×10^{12}	29.17	10×10^{6}	9.17×10^{5}					
360	46.7×10^{12}	52.5	15×10^{6}	23.2×10^{5}					
E_a (kJ/mol)	90.7	84.8	111						
A_0	1.61×10^{9}	1.61×10^{2}	2.65×10^{5}						
5Ni/γ-Al_2O_3, Model of Jeništová et al.[25] (Figure 1i)									
temperature (°C)									
300	2.6×10^{-10}	7.18×10^{-2}	1.3×10^{-10}						
5Ni−Y−H-80, Model of Jeništová et al.[25] (Figure 1i)									
temperature (°C)									
300	2.3×10^{-10}	1.04×10^{-2}	5.26×10^{-8}						
5Ni/SiO_2, Model of Jeništová et al.[25] (Figure 1i)									
temperature (°C)									
300	3.08×10^{-7}	7.46×10^{03}	9.1×10^{-11}						
Pd/C, Model of Jeništová et al.[25] (Figure 1i)									
temperature (°C)									
300	7.7×10^{-11}	4.83×10^{-2}	4.3×10^{-10}						
Ni−H−Y-80, Model of Hachemi et al.[26] (Figure 1j) (C_{18})									
temperature (°C)									
300	8.58×10^{-3}	1.24×10^{-2}	1.34×10^{-2}	1.82×10^{-4}	1.67×10^{-4}	1.25×10^{-3}	3.48×10^{-2}	2.83×10^{-1}	1.29×10^{-2}
Pd/C, Model of Hachemi et al.[26] (Figure 1j) (C_{18})									
temperature (°C)									
300	6.08×10^{-3}	7.08×10^{-3}	1.03×10^{-2}	3.35×10^{-5}	3.17×10^{-5}	4.22×10^{-6}	1.48×10^{-2}	1.97×10^{-1}	1.24×10^{-3}

DOI: 10.1021/acs.energyfuels.8b00947
Energy Fuels 2018, 32, 7245−7261

Table 2. continued

	Kinetic Parameters (s^{-1})								
	k_1	k_2	k_3	k_4	k_5	k_6	k_7	k_8	k_9
Ni−H−Y-80, Model of Hachemi et al.[26] (Figure 1k) (C_{16})									
temperature (°C)									
300			5.0×10^{-3}	8.35×10^{-4}	8.33×10^{-5}	7.08×10^{-4}	1.9×10^{-2}	1.67×10^{-1}	1.0×10^{-2}
Pd/C, Model of Hachemi et al.[26] (Figure 1k) (C_{16})									
temperature (°C)									
300			4.17×10^{-3}	2.72×10^{-5}	1.67×10^{-5}	2.22×10^{-6}	2.03×10^{-3}	1.33×10^{-1}	3.0×10^{-5}

[a]Values shown in italic font have units of s^{-1} Pa. All other values have units as indicated in the table.

unsupported CoMoS catalyst. The experimental results and calculated kinetic parameters using the power law (Table 2) showed that glycerides are quickly decomposed to fatty acids through desterification reactions. Fatty acids are continuously converted into alkanes and other products through either reaction to form alcohols/aldehydes as intermediate products, which proceed via HDO or decarbonylation/decarboxylation reactions (Figure 1d). Through this scheme and kinetic parameters, it is concluded that decarbonylation/decarboxylation reactions (DC_x) were predominant to eliminate O atoms. In addition, during HDO of fatty acids, it seems that alcohol formation prevailed as an intermediate product, as shown in Figure 1e, since the reaction rate coefficient for alcohol formation (k_4) is much higher than that of aldehyde formation (k_3). In addition, polymerization and cyclization reactions occur in parallel.

Bie et al.[20] developed a reaction network during the HDO of methyl heptanoate on Rh/ZrO_2 catalyst. The simplified route shown in Figure 1f was modeled by both power-law and mechanistic models. According to the power-law model, six reaction steps for reaction j and reactant concentration of species i are written considering hydrogen pressure and its corresponding reaction order as follows:

$$r_j = k_j C_i P_{H_2}^{\ m_j} \tag{4}$$

Only eq 5 is considered to be reversible and includes an equilibrium constant k_{eq}, which is temperature-dependent and represented by the van't Hoff equation:

$$r_5 = k_5 C_B C_C - \frac{C_D C_{H_2O}}{k_{eq}} \tag{5}$$

$$k_{eq} = 0.338 \exp\left(\frac{1136}{RT}\right) \tag{6}$$

The model considers the surface reaction mechanism where adsorption is assumed to be competitive or noncompetitive in two different types of active sites. One catalytic site mechanism performs the adsorption of oxygenated species, while the other enhances dissociation of hydrogen molecule.

The molar balance of each species n_i in both gas and liquid fractions is expressed by the following batch reactor model:

$$\frac{dn_i^G}{dt} = -V_R N_{GL,i} a_{GL} \tag{7}$$

$$\frac{dn_i^L}{dt} = WR_i V_L + V_R N_{GL,i} a_{GL} \tag{8}$$

where V_R is the effective reactor volume, V_L the effective liquid-phase volume, and W the mass of catalyst. R_i is the reaction rate of each species i, based on reaction stoichiometry; this component is defined as

$$R_i = \sum \nu_{ij} r_j \tag{9}$$

where r_j is the reaction rate of each step j developed by surface reaction mechanisms. Finally, $N_{GL,i}$ represents the mass-transfer flux at the gas/liquid interface, and a_{GL} is the specific area, which is calculated using the two-film theory:

$$N_{GL,i} a_{GL} = \frac{\frac{C_{G,i}}{K_i'} - C_{L,i}}{\frac{1}{k_{L,i} a_{GL}} + \frac{1}{k_{G,i} a_{GL} K_i'}} \tag{10}$$

$C_{G,i}$ denotes the molar concentration of each component i in the gas phase, $C_{L,i}$ represents the molar concentration of each component i in the liquid phase, K_i' is the modified thermodynamic phase equilibrium ratio, and $k_{L,i}$ and $k_{G,i}$ are the mass-transfer coefficients in the liquid and gas films, respectively.

Even though both models predict successfully the kinetic behavior of reactants and products species, the mechanistic model outperformed the power-law model. This is due to some species with low concentration increases mathematical deviations compared with species with high concentration. However, both mechanistic models better fitted the experimental data with a similar order of magnitude.

In addition, the effect of hydrogen pressure on methyl heptanoate conversion was studied, being negligible, compared with reaction temperature. However, it was observed that increasing the pressure of hydrogen slightly improves the hydrogenation reaction of heptanoic acid toward heptanol.

In another study, Bie et al.[21] used Rh/ZrO_2 catalyst during HDO of methyl palmitate. The authors explain the bifunctionality of catalysts based on noble/transition metals in their reduced state as active sites to perform the dihydrogen activation via dissociative adsorption; similarly, oxygen vacancy sites on the support (ZrO_2) work as active sites for the oxygenated species. Similar to other model compounds studied, the first reaction performed is hydrogenolysis. In this case, palmitic acid and methane are produced as shown in Figure 1g. The rate equations of the key reaction steps were obtained by a similar mechanistic model previously employed for each of the reactions, only for the reaction rate (r_1), a slight modification was made by adding the hydrogen concentration to better describe the effect of the pressure on the reaction kinetics.

$$r_1 = \frac{k_1 C_A \sqrt{K_{H_2} C_{H_2}}}{\left(1 + \frac{K_B C_B}{\sqrt{K_{H_2} C_{H_2}}} + \frac{K_C C_C}{\sqrt{K_{H_2} C_{H_2}}}\right)\left(1 + \sqrt{K_{H_2} C_{H_2}}\right)} \tag{11}$$

Nevertheless, reaction rates 2 and 3 (r_2 and r_3, respectively) follow the same mechanism hypothesis reported,[20] which share

DOI: 10.1021/acs.energyfuels.8b00947
Energy Fuels 2018, 32, 7245−7261

a common rate of determination step (the final addition of a hydrogen atom in the reactant species):

$$r_j = \frac{k_j K_B K_{H_2} C_B C_{H_2}}{\left(1 + \frac{K_B C_B}{\sqrt{K_{H_2} C_{H_2}}} + \frac{K_C C_C}{\sqrt{K_{H_2} C_{H_2}}}\right)(1 + \sqrt{K_{H_2} C_{H_2}})} \quad (12)$$

Finally, reaction rate r_4 considers the reversible dehydrogenation−decarbonation of hexadecanol in pentadecane:

$$r_4 = \frac{k_4 K_C C_C}{\left(1 + \frac{K_B C_B}{\sqrt{K_{H_2} C_{H_2}}} + \frac{K_C C_C}{\sqrt{K_{H_2} C_{H_2}}}\right)(K_{H_2} C_{H_2})} \quad (13)$$

The kinetic model developed can be adequately fitted to experimental data on a wide range of reaction conditions and conversions, unlike other models based on power-law kinetics.

Recently, the HDO of triglycerides was investigated using a mixture of tripalmitin (TP) and tristearin (TS) in a batch reactor over a Ni/Al_2O_3.[22] The study was performed using a 1:2 molar mixture ratio of TP:TS at temperatures ranging from 280 °C to 360 °C and 5−20 wt % catalyst loading. The HDO experiments showed that TP and TS were converted instantaneously to fatty acids and propane. It agrees with results reported by Zhang et al.,[23] who found high rate of triglyceride decomposition. The scheme presented in Figure 1h shows the kinetic model based on the experimental results where oxygen removal routes prevail.

Conversion of triglycerides occurs by conversion of them to aldehydes and then to alcohols as intermediate products to finally produce alkanes and water through reduction/dehydration reactions, which proceed in unsaturated sites of sulfhydryl groups formed in the catalyst that is performing the hydrogenation. In sulfide catalysts such as Ni or CoMo, H_2S (or a sulfur-containing compound of easy decomposition) is added to the feedstock to preserve their activity. The presence of H_2S in the feedstock also plays a role in reaction selectivity. In the absence of H_2S in the feed, the DDO/HYD selectivity is high; however, this ratio diminishes as H_2S is added by which inhibition effect of hydrogen sulfide is attained in DDO pathway than in the HYD route, as reported elsewhere.[24]

Because of the fact that Ni/Al_2O_3 catalyst is weakly acidic, the alkane production is enhanced by decarbonylation reactions. The reaction rates were expressed by the power-law model, assuming a first-order reaction, with respect to compounds in liquid phase and considering the hydrogen partial pressure (P_{H_2}) during hydrogenation reactions. In the case of stearic or palmitic acid (A), the reaction rate is defined as

$$-\frac{dC_A}{dt} = k_1 C_A P_{H_2} \quad (14)$$

The model takes into account conversion of aldehydes (B) to alcohols (D) as a reversible reaction, so that the equilibrium constant (k_{eq}) was included.

$$\frac{dC_B}{dt} = k_1 C_A P_{H_2} - k_2 C_B - k_3 C_B P_{H_2} + \left(\frac{k_3}{k_{eq}}\right) C_B \quad (15)$$

$$\frac{dC_D}{dt} = k_3 C_B P_{H_2} - \left(\frac{k_3}{k_{eq}}\right) C_D - k_4 C_D \quad (16)$$

To determine the precise hydrogen partial pressure at any reaction time, it is necessary to subtract the amount of stoichiometric hydrogen consumed by Tg, C, D, and E, according to the following equation:

$$P_{H_2} = P^0_{H_2} - \frac{V_L(3C_{Tg,0} + C_C + 2C_D + 3C_E)R_u T}{V_G} \quad (17)$$

where V_L and V_G are the volume of liquid and gas, respectively. Kinetic parameters are shown in Table 2. The results of kinetic coefficients show that decarbonylation reaction (k_2) predominates over the HDO reaction (k_3). Moreover, rate coefficients k_1, k_2, and k_3 for both triglyceride types showed similar values and only k_4 is slightly different.

Jenišťová et al.[25] carried out a study to investigate the influence of hydrogen pressure on the HDO of stearic acid and tall oil fatty acids (TOFA). It was shown that, the higher the hydrogen pressure, the higher the fatty acid conversion. Experiments were carried out in a semibatch reactor over a reduced $Ni/\gamma\text{-}Al_2O_3$ at 300 °C, varying the hydrogen pressure from 7 bar to 30 bar. The reaction mechanism is similar to previous studies reported elsewhere,[19] with some differences in the paths in which oxygen atoms are subtracted, as observed in Figure 1i. The authors carried out tests without performing the prereduction of the catalyst, concluding that, with a prereduction step, much higher conversion of stearic acid was obtained, including greater selectivity of C_{17} products. The reaction rate is expressed by the Langmuir−Hinshelwood model, taking into account the effect of hydrogen pressure only for hydrogenolysis reactions (1 and 3). Each reaction rate is assumed as noncompetitive adsorption of hydrogen and organic species. For instance, the rate for reaction (r_1) is

$$-r_1 = \frac{k_1' C_A P_{H_2}}{(1 + K_A C_A)(1 + K_H P_{H_2})} \quad (18)$$

Different catalysts (Ni−H−Y-80, Ni/SiO_2, Pd/C) were used for the HDO of steric acid, and the kinetic parameters show that DC_x reactions predominated in all cases, as observed in Table 2. The authors evaluated the hydrotreatment of these feeds at 300 °C and 30 bar over 5 wt % Ni−H−Y-80 and 5 wt % Pd/C catalysts. Regardless of the feed type, characterization analyses showed the presence of C_{16} and C_{18} as the most abundant products. Kinetic models developed for C_{18} and C_{16} are depicted in Figures 1j and 1k, respectively. The results indicate that molecules with different numbers of carbon atoms undergo similar steps. Based on these models, reaction rate equations were developed using the Langmuir−Hinshelwood mechanism, considering that the absorption of acid species A is significantly much greater than those of the other species (aldehydes, alcohols, alkanes, etc.). For instance, the reaction rate equation of methyl linoleate is expressed as

$$\frac{dC_{Mln}}{dt} = -\frac{k_1 C_{Mln}}{(1 + K_A C_{SA})} \quad (19)$$

Kinetic parameters show that the HDO reaction ($k_6 > k_5$) predominates with Ni-based catalyst, whereas, in the Pd catalyst, the reactions of DC_x ($k_5 > k_6$) are present. On the other hand, it was found that, for both catalysts, the values of kinetic parameters are dependent on the carbon chain length in the feed.

Kinetic studies for HDO developed with model compounds have generated a great variety of kinetic models, because of the diversity of reaction mechanisms that occur due to the great complexity of feeds, many types of catalysts, and variety of

DOI: 10.1021/acs.energyfuels.8b00947
Energy Fuels 2018, 32, 7245−7261

operating conditions to be used. Most of them fall into similar conclusions, where the molecules of triglycerides and fatty acids ester undergo instantaneous reactions of hydrogenolysis to form intermediate acid compounds.[26] Depending on these parameters, it is possible to remove O atoms through HDO, decarboxylation, and/or decarbonylation.

Other kinetic models based on functional groups of oxygenated compounds in the solvolytic primary oil and relative gaseous product determined by infrared spectroscopy by Fourier transform were developed.[27,28] Experimentation was carried out at 300 °C and 8 MPa on different catalysts ($NiMo/Al_2O_3$, Pd/C, and MoS_2) and different activation states (oxidized, reduced and sulfided). The model presented in Figure 2e considers the

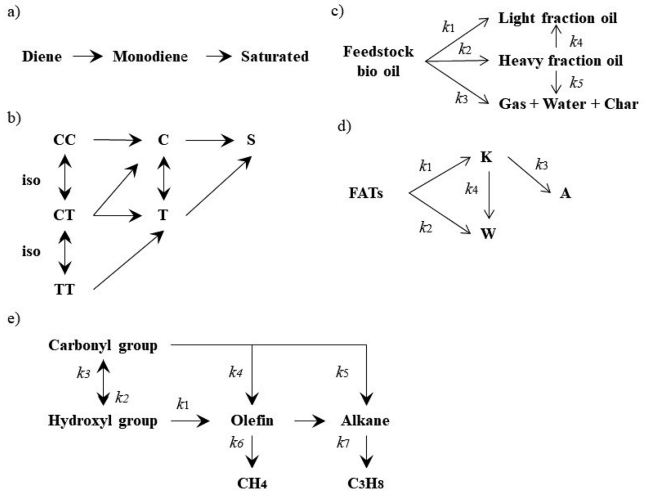

Figure 2. Reaction pathways for the hydrotreatment of bio-oils.

conversion of the species with hydroxyl and carbonyl functional groups to gaseous products to form olefins and alkanes. The reaction rate equations were developed based on the relative concentration of these oxygenated compounds y_i (i = OH, C═O, CHO, CO, CO_2, H_2O, CH_3, and C_3H_8), and an apparent constant of reaction product of the intrinsic rate constant and internal effectiveness factor:

$$r_j = k_j y_i \tag{20}$$

$$y_i = \frac{C_i}{C_{OH(t=0)}} \tag{21}$$

Experimental results show that catalysts in the form of oxides exhibited a greater selectivity toward DCx reactions among all the catalysts evaluated. However, the hydrocracking reactions were considered to be negligible. It is observed that the activity and selectivity of these catalysts were maintained during the reaction time without regeneration. On the other hand, catalysts in reduced form exhibited deoxygenation activity similar to that of the oxidized form. However, the reactions of DCx reaction showed inhibition effects. Finally, the catalysts in the sulfided form showed the highest affinity for hydrocracking reactions, while the decarbonylation was completely inhibited. In the same way, the MoS_2 catalyst showed high activity and selectivity for HDO. Ni- and Mo-based sulfide catalysts presented higher activity for all investigated reactions, compared to Pd catalysts.

Based on a similar model, the effect of the reaction temperature, hydrogen pressure, stirring speed, and heating rate during the solvolytically liquefied hydrotreatment was studied in a $NiMo/Al_2O_3$ catalyst, with tetralin as a hydrogen donor. The results showed that, at 225 °C, removal of hydroxyl groups appeared, which was easier to remove than carboxyl groups. Stirring speed and heating rate had a negligible effect.

2.2. Real Feeds. When working with complex systems such as bio-oils, the kinetic models are typically represented by grouping compounds with similar properties in the so-called lumps. In this way, a large number of parameters can be reduced and the effects of process variables on products yield can be quantified. Fernandez et al.[29] proposed two kinetic models to describe the performance during the hydrogenation of unsaturated compounds in sunflower oil. The first one describes the hydrogenation of linoleic acid (diene) to produce oleic acid (monodiene), which reacts to form stearic acid (saturated). This considers the formation of a half-hydrogenated surface intermediate (Figure 2a). The second one is a model that incorporates the *cis*−*trans* (C-T) isomerization reactions including a semihydrogenated intermediate and the Horiuti−Polanyi mechanism (Figure 2b). All experiments were performed in a semibatch reactor with Pd catalyst in a temperature range of 80−120 °C and reaction pressure between 2 bar and 3 bar. The results showed that activation energies of dienes (49−58 kJ/mol) are higher than those for monoene (40−46 kJ/mol) and approximately similar for the isomerization step (55−60 kJ/mol).

Zhang et al.[30] reported a kinetic model for bio-oil HDT based on the distribution of distillation curves of products. Figure 2c represents the reaction scheme indicating bio-oil and HDT products: light fraction (<250 °C), heavy fraction (250−450 °C), and byproducts (gas−water-char) as single lumps. The power-law-based kinetic model is represented by irreversible first-order rate equations (eqs 2 and 3). The values obtained of activation energies and pre-exponential factors are shown in Table 3.

Selishcheva et al.[31] studied the hydroconversion of rapeseed oil fatty acid triglycerides (FATs) over nonsulfided nickel catalysts ($NiCu/CeO_2$−ZrO_2). A kinetic model was developed in a flow fixed-bed reactor under temperatures of 300−380 °C, 10 bar of hydrogen pressure, and a liquid hourly space vecolity (LHSV) of 0.38−0.1 h^{-1}. The model groups the FATs as a single lump and their products into three lumps: group W, which contains heavy molecular oxygenates such as ketones and waxes; group K, which consists of oxygen-containing compounds (mainly free fatty acid, alcohol, and aldehydes of low molecular weight); and group A, which is comprised of only alkanes. The corresponding scheme is represented in Figure 2d. Based on the selectivity and products distribution in each group, some kinetic parameters were determined as observed in Table 3. It was concluded that, at any temperature, the formation rate of alkanes predominates over the formation of oxygenated compounds, because the former exhibited the lowest activation energy.

Another kinetic model was developed for the hydrotreatment of Jatropha oil in the presence of a CoMo/MTS catalyst. Sharma et al.[32] described the conversion of triglycerides present in Jatropha oil as a single lump at 300−320 °C, considering different possible reaction pathways and their conversion toward light compounds (C_5−C_8), middle compounds (C_9−C_{14}), heavy compounds (C_{15}−C_{18}), and oligomeric compounds (>C_{18}). The fitted reaction model is depicted in Figure 3, and Table 3 shows the values of the reaction rate coefficients.

The kinetic model shows that triglycerides do not produce only deoxygenation compounds (heavier and oligomerized

DOI: 10.1021/acs.energyfuels.8b00947
Energy Fuels 2018, 32, 7245−7261

Table 3. Kinetic Parameters Determined during the HDO of Bio-oil

	Kinetic Parameters (h^{-1})										
	k_0	k_1	k_2	k_3	k_4	k_5	k_6	k_7	k_8	k_9	k_{10}
Model of Zhang et al.[30] (Figure 2c)											
E_a (kJ/mol)		64.81	75.44	66.281	97.12	27.88					
A_0		1.29×10^5	1.32×10^6	5.74×10^4	1.51×10^7	2.57×10^2					
$NiCu/CeO_2-ZrO_2$, Model of Selishcheva et al.[31] (Figure 2d)											
temperature (°C)											
300		0.49	0.01	7.55	0.55						
320		0.95	0.05	12.1	0.9						
340		1.49	0.11	11.2	1.5						
360		2.97	0.33	15	1.3						
380		5.1	0.9	17	1.8						
E_a (kJ/mol)		89.4	167.6	28.3	42.7						
A_0		6.9×10^7	2.3×10^{13}	3.1×10^3	4.9×10^3						
CoMo/MTS, Model of Sharma et al.[32] (Figure 3)											
temperature (°C)											
300	7.39	7.27	0.07	0.02	0.03						
320	14.35	13.25	1.24	0.11	0.04						
$CoMo/Al_2O_3$, Model of Anand and Sinha[33] (Figure 3)											
temperature (°C)											
320	17	7	10						0.3	0.3	
340	17	13	3	0.2	1.1	5			0.4		3
360	24	2	19	2	1				0.1		0.1
E_a (kJ/mol)	26	87	43	127	47						
A_0	31.9×10^2	14.5×10^4	62.6×10^5	4.2×10^{10}	13.7×10^4						
$NiW/SiO_2Al_2O_3$, Model of Anand et al.[35] (Figure 3)											
temperature (°C)											
340	1.06	0.2	0.84						0.04	0.04	
420	23.4	2.7	18.8	1.2	0.6				0.2	0.1	0.1

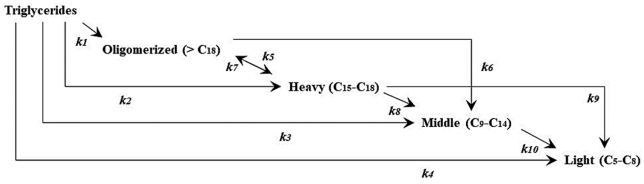

Figure 3. Reaction pathways for the hydroconversion of triglycerides.

compounds). They are also converted to lighter and middle compounds under these temperatures. The generation of smaller alkanes is attributed to high acidity of the catalyst, promoting cracking reactions. However, it is important to emphasize that experimental data lead to only primary reactions and the rate of oligomerization is much higher, compared with other reactions. Authors indicated that oligomeric products, which form coke, have a tendency to accumulate on the catalyst surface. Note that the model does not consider a pathway for gas formation. The reaction rate coefficients indicate that reaction rate of triglycerides to oligomerized products predominates, being much higher than others. Moreover, there is an increase, by a factor of 20, in the reaction rate coefficients for the production of heavy compounds as the temperature increases from 300 °C to 320 °C.

Anand and Sinha[33,34] reported another set of kinetic pathways, considering all possible reaction products during hydroconversion and oligomerization of triglycerides in Jatropha oil in different reaction mechanisms. However, in order to facilitate the determination of reaction rate coefficients with less computation time, a general model including all reaction steps was proposed (see Figure 3). The experimentation was performed with $CoMo/\gamma\text{-}Al_2O_3$ catalyst in a temperature range of 320−360 °C at a pressure of 80 bar. The results showed that, at low temperature (320 °C), triglycerides undergo consecutive side reactions, having naphtha and kerosene compounds as secondary products (C_5-C_8 and C_9-C_{14}, respectively) in low proportion, because of the lower acidity and metal support interaction, compared with the CoMo/MTS catalyst reported by Sharma.[32] On the other hand, at mild temperature (340 °C), lighter compounds were observed, because, at this temperature, thermal cracking influences all lumps. In addition, diesel ($C_{15}-C_{18}$) and kerosene (C_9-C_{14}), as well as nonstable oligomerized compounds, are subjected to cracking reactions. Finally, at 360 °C, similar pathways are followed, yielding stable oligomerized products. The kinetic parameters obtained for each sequence of reactions are presented in Table 3, showing the influence of temperature on the hydrotreatment of bio-oil. Anand et al.[35] conducted a kinetic and thermodynamic study on the hydrotreatment of Jatropha oil to determine the diffusion limitations, kinetic reaction mechanisms, and thermodynamics, using $NiW/SiO_2-Al_2O_3$ catalyst in a fixed-bed microreactor. The study considered all reaction pathways, as shown in Figure 3. The results indicate that below 340 °C, triglycerides undergo the same kinetic mechanisms and the reaction rate coefficients have similar tendencies as those reported by Anand and Sinha[33] with $CoMo/Al_2O_3$ as a catalyst at 320 °C. On the other hand, at high temperature (420 °C), the reaction rate changes slightly, because diesel is also converted to a naphtha fraction, as a consequence of the presence of acidic sites. The authors also concluded that inner diffusion was negligible, since the effectiveness factor was ∼1.

Velez[36] studied the reaction pathway of palm oil triglycerides in a TBR using $NiMo/\gamma\text{-}Al_2O_3$ catalyst at temperatures of

DOI: 10.1021/acs.energyfuels.8b00947
Energy Fuels 2018, 32, 7245−7261

335−350 °C, a pressure of 60 bar, and a residence time of 15−60 min, and the product was mainly formed by C_{15}−C_{18}-saturated compounds. This model assumes that fatty acids in triglycerides have the same number of carbons. The simplified model of reactions and kinetic equations are presented in Table 4, which

Table 4. HDO Pathways Used for the Estimation of the Kinetic Parameters

catalyst	reaction	reaction rate
Hydrogenation of Unsaturated Triglycerides		
Trilinolein (LLL)	$C_{57}H_{98}O_6 + 6H_2 \rightarrow C_{57}H_{110}O_6$	$r_1=k_1C_{OOO}$
Triolein (OOO)	$C_{57}H_{101}O_6 + 3H_2 \rightarrow C_{57}H_{110}O_6$	$r_2=k_2C_{LLL}$
Hydrodeoxygenation		
Tripalmitin (PPP)	$C_{51}H_{98}O_6 + 12H_2 \rightarrow 3C_{16}H_{34} + C_3H_8 + 6H_2O$	$r_3=k_3C_{PPP}$
Tristearin (SSS)	$C_{57}H_{110}O_6 + 12H_2 \rightarrow 3C_{18}H_{38} + C_3H_8 + 6H_2O$	$r_4=k_4C_{SSS}$
Hydrodecarboxylation		
Tripalmitin (PPP)	$C_{51}H_{98}O_6 + 3H_2 \rightarrow 3C_{15}H_{32} + C_3H_8 + 3CO$	$r_5=k_5C_{PPP}$
Tristearin (SSS)	$C_{57}H_{110}O_6 + 3H_2 \rightarrow 3C_{17}H_{36} + C_3H_8 + 3CO$	$r_6=k_6C_{SSS}$

takes into account a first-order reaction and acceptable determination coefficient (R^2 = 0.80). However, concentration values have a tendency to be underestimated when mild reaction conditions are used.

In addition to the aforementioned models, kinetic studies have been focused on hydrotreating of bio-oil,[37,38] biomolecules,[8,39] and even cohydroprocessing of these with petroleum derivatives[40,41] to determine an overall reaction rate where lumping is the most common way to establish the pathway reaction. Table 5 shows different reaction rate equations based on power law, Eley−Rideal, and Langmuir−Hinshelwood models for palmitic acid HDO.

Most of the kinetic studies focus on intrinsic kinetics (mass-transfer-free kinetics), which gives an accurate idea of the physical and chemical phenomena that are happening. However, if possible, it is recommended to perform tests to minimize diffusional effects based on the smallest number of assumptions as possible. In addition, the kinetic model can be properly used in a reactor model later. On the other hand, few studies take into account the use of statistical techniques to ensure that estimated kinetic parameters provide the greatest possible convergence to experimental data. Figure 4 shows a general

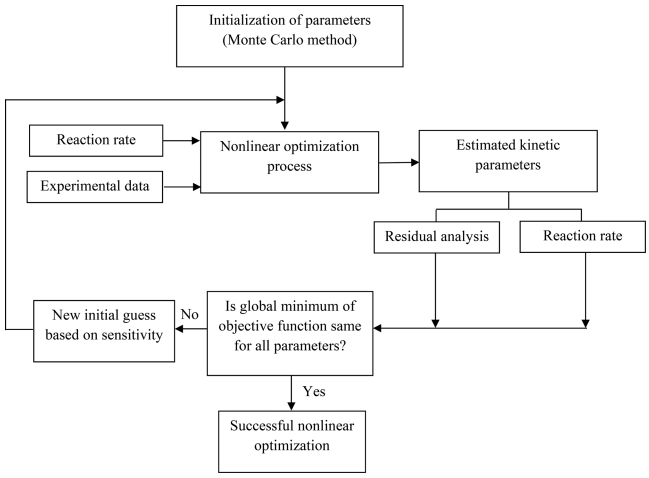

Figure 4. General approach for optimization of parameter values of kinetic models.

algorithm involving different steps such as initial guesses, nonlinear parameter estimation, and parameter sensitivity analysis to ensure that the obtained values are properly estimated and the global minimum of the objective function is obtained.[42]

2.3. Catalysts. The role of catalysts and catalytic sites have been reported based on model compounds. For example, Al_2O_3-supported CoMo and NiMo sulfide catalysts were used

Table 5. Expressions of Reaction Rate from Different Models

model	expression	details
power law	$r_{PA} = -k_{rxn}C_{PA}{}^{n}P_{H_2}{}^{m}$ $k_{rxn} = A_0\ e^{E_a/(RT)}$	
Eley−Rideal	$r_{PA} = -\frac{k_{rxn}C_{PA}P_{H_2}}{1 + K_{H_2}P_{H_2}}$	Nondissociative adsorption of H_2
	$r_{PA} = -\frac{k_{rxn}C_{PA}\left(P_{H_2}\right)^{0.5}}{1 + \left(K_{H_2}P_{H_2}\right)^{0.5}}$	Nonadsorbed PA Dissociative adsorption of H_2 Nonadsorbed PA
Langmuir−Hinshelwood	$r_{PA} = -\frac{k_{rxn}K_{PA}C_{PA}K_{H_2}P_{H_2}}{(1 + K_{PA}C_{PA})(1 + K_{H_2}P_{H_2})}$	Dual site adsorption Nondissociative adsorption of H_2 Nondissociative adsorption of PA
	$r_{PA} = -\frac{k_{rxn}C_{PA}P_{H_2}}{(1 + K_{PA}C_{PA})(1 + (K_{H_2}P_{H_2})^{0.5})^2}$	Dual site adsorption Dissociative adsorption of H_2 Nondissociative adsorption of PA
	$r_{PA} = -\frac{k_{rxn}C_{PA}P_{H_2}}{(1 + K_{PA}C_{PA} + K_{H_2}P_{H_2})^2}$	Single site adsorption Nondissociative adsorption of H_2 Nondissociative adsorption of PA
	$r_{PA} = -\frac{k_{rxn}C_{PA}\left(P_{H_2}\right)^{0.5}}{(1 + K_{PA}C_{PA} + \left(K_{H_2}P_{H_2}\right)^{0.5})^2}$	Single site adsorption Dissociative adsorption of H_2 Nondissociative adsorption of PA

DOI: 10.1021/acs.energyfuels.8b00947
Energy Fuels 2018, 32, 7245−7261

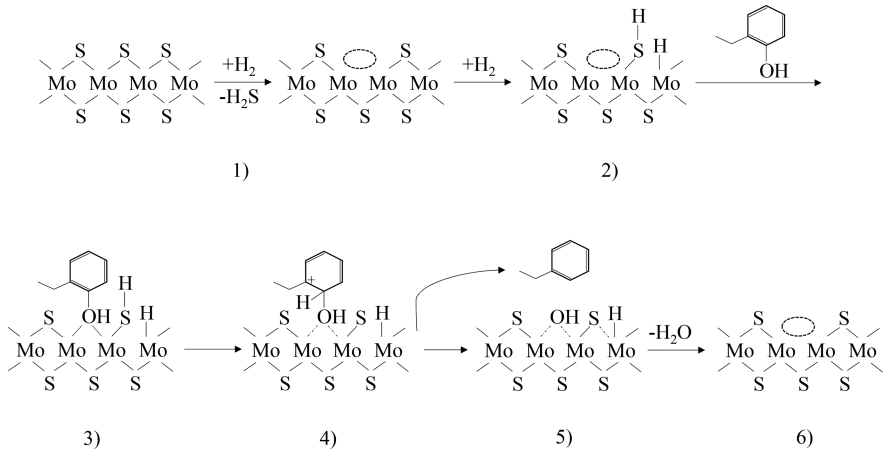

Figure 5. DDO mechanism on unpromoted MoS_2 catalyst using 2-ethylphenol as a model molecule.

in 4-methylphenol HDO. The sulfide state was preserved during reaction by adding CS_2 to the feedstock. $NiMo/Al_2O_3$ catalyst was more active than $CoMo/Al_2O_3$ and the hydrogenation-to-direct deoxygenation (HYD/DDO) ratio was higher when using NiMo as a catalyst, as reported by Laurent and Delmon,[43] which indicates that NiMo catalyst enhanced hydrogenation reaction. On the other hand, $CoMo/Al_2O_3$ was more active than $NiMo/Al_2O_3$ during phenol HDO, as reported elsewhere.[44]

Romero et al.[45] studied the conversion of 2-ethylphenol (2-EtPh) on alumina, Mo/Al_2O_3, $CoMo/Al_2O_3$, and $NiMo/Al_2O_3$. Alumina enhances disproportionation and isomerization reactions due to acidity of support. When Mo/Al_2O_3 in the sulfide state was used, deoxygenated products were obtained. Catalytic activity when using sulfide catalysts is attributed to coordinatively unsaturated sites (CUS) acting as Lewis acid sites and as an approach to 2-ethylphenol deoxygenation mechanism, it is assumed that vacancies are on metallic edges of MoS_2 slabs. On these vacancies, HYD and DDO products are ready to be formed. However, differences among adsorption mode would occur, i.e., in the DDO pathway, the adsorption of 2-EtPh happens through the O atom, whereas in HYD, pathway adsorption is flat through the aromatic ring. In the case of the DDO pathway, the authors have depicted the reaction mechanism as follows: (1) in the presence of hydrogen, a vacancy is formed as H_2S is subtracted; (2) heterolytic dissociation of hydrogen forms S−H and Mo−S groups, which are attached to adjacent Mo atoms; (3) a molecule of 2-EtPh is adsorbed through its O atom in the vacancy; (4) a proton from the S−H group is added to the adsorbed molecule, which turns into a carbocation; (5) the carbocation is stabilized by C−O cleavage (at this stage, a deoxygenated compound is obtained); and (6) the vacancy is recovered by water elimination. Figure 5 shows the proposed mechanism.

In the case of HYD route, adsorption of oxygenated molecules occurs through the flat aromatic ring, which could involve more space, such as neighboring vacancies. This fact would imply that the HYD route were catalytically limited, when compared with DDO; however, higher HYD activity than DDO activity has been observed in some cases, because of not only vacancies on the MoS_2 slabs that are present but also brim sites on the basal planes of MoS_2 slabs, which enhance hydrogenation, as reported elsewhere.[45,46]

When Ni or Co are used as promoters, catalytic activity is increased by electron donation to Mo, causing the cleavage of the metal−sulfur bond, as reported by Chianelli.[47] The presence of cobalt develops the so-called CoMoS crystallites having hexagonal geometry, whereas Ni enhances the NiMoS crystallites to be deformed hexagons. Cobalt has a tendency to deposit on sulfur edges while nickel has an affinity for metallic edges. HYD pathway of 2-EtPh is enhanced by NiMo catalysts, while DDO predominates on CoMo catalysts.[45]

When no hydrotreating catalysts (sulfide catalyst) are used, such as transition-metal phosphides, the HDO reaction proceeds particularly through metal sites that have both Lewis and metallic properties. Small and positive charges on metals ($M^{\delta+}$), such as Ni and Mo, are observed and considered as Lewis acid sites involved in hydrogenolysis, demethylation, and hydrogenation reactions. In addition, Brønsted sites (PO−H groups) provide hydrogen to catalyze hydrogenation and hydrogenolysis reactions; however, less activity of these sites was observed, compared with metal sites.[48] HDO on transition-metal phosphides is depicted when the oxygen-containing molecule and hydrogen are adsorbed and activated on metal sites, then H atoms from metal and Brønsted sites react with intermediate species containing oxygen to finally produce oxygen-free compounds.[4]

3. MODELS FOR CATALYTIC DEACTIVATION

One of the main challenges to be overcome during the hydrotreatment of vegetable oils is catalyst deactivation. It is argued that the main cause of deactivation is coke deposition. However, it has been identified that compounds with O atoms have a higher affinity to coke formation through polymerization reactions. Sebos et al.[40] studied the coprocessing of cottonseed oil with desulfurized petroleum diesel and an activity function (α) was included in the HDO rate equation. This parameter is defined as the ratio of reaction rate coefficient at any time t, with respect to that at the reference time, as follows:

$$\alpha = \frac{k_{\mathrm{HDO}_t}}{k_{\mathrm{HDO}_{\mathrm{ref}}}} \tag{22}$$

The activity function was considered to determine the deactivation rate during the HDO of waste cooking oil.[19] The model was applied to calculate the deactivation rate of both HDO and DC_x routes by means of specific decay constants k_{d1} and k_{d2}, respectively. The decay rate follows a second-order law, with respect to the activity parameter.

$$\frac{\mathrm{d}\alpha_j}{\mathrm{d}t} = k_{\mathrm{d}_j}\alpha_j^{\,2} \tag{23}$$

DOI: 10.1021/acs.energyfuels.8b00947
Energy Fuels 2018, 32, 7245−7261

The sum of both decay constants (k_{d1} and k_{d2}) provides the total deactivation rate, which indicated a loss of activity of 80% at the end of the reaction. The results showed that the DC_x route contributed mainly to deactivation (k_{d2} = 0.4475), while the HDO route had no significant effect ($k_{d1} \approx 0$).

During guaiacol HDO, a catalyst deactivation parameter α is proposed as well,[40] which is a function of product concentration (C_B), causing catalyst deactivation, and a temperature-dependent parameter (γ) that determines the concentration at which the reaction decreases.

$$r_i = \alpha k C_i {P_{H_2}}^m \tag{24}$$

$$\alpha = 1 - \gamma C_B \tag{25}$$

The parameter γ is a linear function of temperature and two constants c_1 and c_2:

$$\gamma = c_1 T - c_2 \tag{26}$$

In addition to polymerization reaction, catalyst deactivation could be enhanced as competence between reactants and intermediates on catalytic acid sites. In another study, Boldrini et al.[49] employed different deactivation models based on the activity function or catalytic deactivation α and the number of reuses of catalyst β, which has a value of 1 for the first use of catalyst.[50]

$$\varphi_1 = \alpha_1 \beta = \beta_0 (1 - ct) \tag{27}$$

$$\varphi_2 = \alpha_2 \beta = \beta_0 \exp(-ct) \tag{28}$$

$$\varphi_3 = \alpha_3 \beta = \frac{\beta_0}{(1 + ct)} \tag{29}$$

The mass balance of C_i considering the overall effectiveness factor (η) and bulk density (ρ_b) can be written as

$$\frac{dC_i}{dt} = \varphi_1 \rho_b \eta \sum \nu_{ij} r_i \tag{30}$$

However, it would be necessary to test this type of deactivation models for the HDO of bio-oils.

4. MODELING OF CATALYTIC REACTORS FOR BIO-OIL CONVERSION

The development of a mathematical model is based on mass and energy balances among different phases in the reacting system (gas, liquid, and solid). In some cases, the momentum balance and pressure drop through the catalytic bed can be considered. A general reactor model considers all the terms of mass- and energy-transfer resistances (between gas−liquid, liquid−solid, intraparticle diffusion, axial and radial diffusion), as well as accumulation, convection, and generation terms of different species.

A complex reactor model requires one to gather enough information about phenomena occurring in the system. For instance, in a fixed-bed reactor, the mass radial dispersion can be neglected if the ratio of reactor-to-particle diameter (d_T/d_P) is higher than 25. If gas and liquid velocities are high enough, the effect of axial dispersion of fluid flow in a commercial fixed-bed reactor can be neglected. A detailed explanation of these terms and other was reported by Mederos et al.[51] The development of a reactor model is dependent on the complexity required. If the model is too complex, it can be difficult to solve; on the other hand, if the model is too simple, it may not converge with experimental data. Therefore, these assumptions, which must be validated with experimental data, are needed.

There are few models to describe the reactor performance during the hydrotreating of vegetable oils. The first models were focused on the hydrogenation of unsaturated compounds present in bio-oils.[52−56] Velez[36] established a conceptual industrial reactor design for hydrotreatment based on experiments with refined, bleached, and deodorized palm oil (RBDPO) by studying two cases on avoiding hot spots higher than 370 °C to control excessive product cracking and considering the flow as ideal. The molar balance equation for compound i considers the temperature and liquid residence time by the kinetic model presented in Table 4 and does not take into account any mass-transfer effect.

$$\frac{dC_i}{dL} = \left(\frac{A\rho_b}{V_0}\right) r_i \tag{31}$$

To consider the exothermal behavior of the HDO reaction, the energy balance was expressed by

$$\frac{dT}{dW} = \frac{U_a(T_a - T) + \sum_{i=1}^{q} (r_{ij})[\Delta H_{ij}]}{\sum_{i=1}^{m} F_i C_{p_i}} \tag{32}$$

and pressure drop was calculated with Ergun equation for packed beds:

$$\frac{dP}{dz} = -\frac{G}{\rho_b d_p} \frac{(1 - \varepsilon)}{\varepsilon^3} \left[\frac{150(1 - \varepsilon)\mu}{d_p} + 1.75G\right] \tag{33}$$

In one case (case a), feedstock and hydrogen are simultaneously injected at the reactor top whereas in the second case (case b), it takes into account a hydrogen-quenching stream close to the reactor inlet. From the energy balance, Figure 6a shows a peak in temperature at 0.55 m, which is due to the energy released by exothermal reactions (mainly reactions 3 and 4 in Table 4). Figure 6b shows that the pressure drop was higher in case b, although it can be considered as negligible in both cases. Case b was considered to be the best option, because the temperature of the liquid increased only 9 °C, which would reduce the catalyst weight by 800 kg to obtain an alkane/RBDPO ratio similar to case 1, as shown in Figure 6c.

Boldrini et al.[49] developed a complex mathematical model for $Pd/Al_2O_3/Al$ monolithic stirrer reactor during the hydrotreatment of sunflower oil where hydrogenation/isomerization reactions are expected to occur. Reaction conditions were explored in the following ranges of temperature and pressure: 80−100 °C and 4.1−5.5 bar, respectively. The mass balance included the overall effectiveness factor (η) and deactivation parameter (α). Moreover, the mass-transfer coefficient (k_{LS}) in the liquid−solid interphase is experimentally determined while the mass-transfer coefficient of hydrogen in the liquid−solid film is calculated using the Sherwood correlation:

$$Sh = \frac{k_{LS} D_H}{D} = 1.16(ReSc)^{1/3} \tag{34}$$

The following energy balance was used for the temperature difference between the fluid and the catalyst surface:

$$(T_s - T_B) = \frac{(-\Delta H_{ij(T)}) R_H W}{h a_m} \tag{35}$$

The heat-transfer coefficient (h) can be calculated using the Nusselt number. To determine the maximum temperature

DOI: 10.1021/acs.energyfuels.8b00947
Energy Fuels 2018, 32, 7245−7261

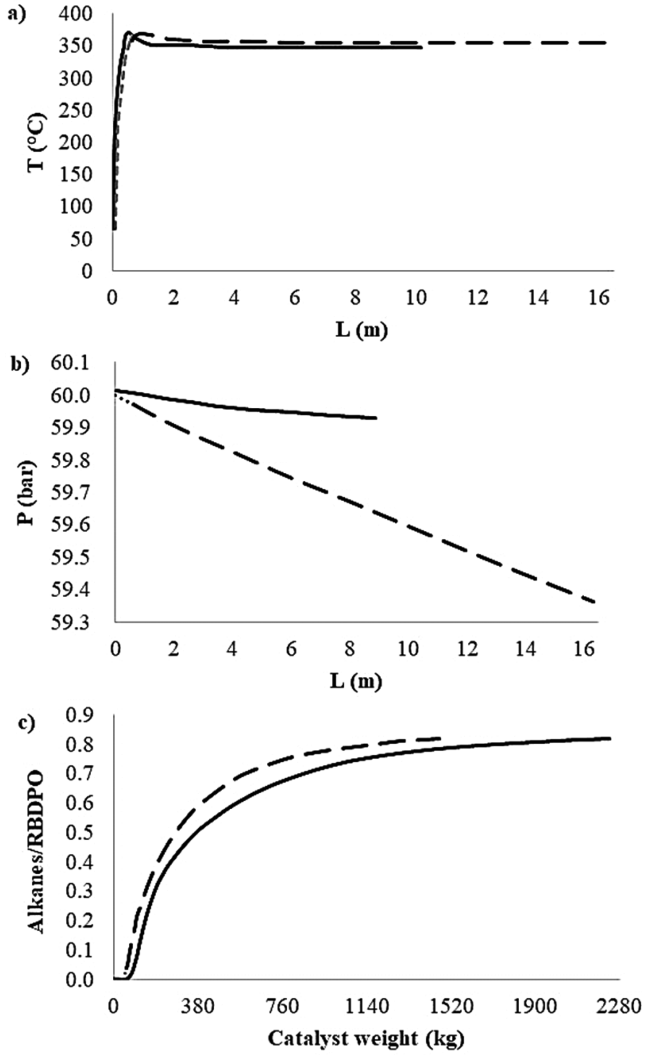

Figure 6. (a) Temperature, (b) pressure drop, and (c) concentration profiles of a palm oil hydrotreating reactor. [Legend: solid line (—) represents data for case 1, dashed line (– – –) represents data for case 2.[36]

gradient inside the catalyst, the following expression was deduced:

$$\Delta T = \frac{(\Delta H_{ij(T)})D_e C_{H_2,S}}{\lambda_e} \tag{36}$$

Through different simulation cases, it was shown that the model could be applied to generate strategies for optimizing the reactor performance, in terms of operating costs.

Forghani et al.[57] developed a two-dimensional mathematical model of a heterogeneous hydrocracking reactor. The trickle-bed reactor model takes into account the two-film theory to obtain the mass- and energy-transfer coefficients. The kinetic models were solved and validated based on literature reports.[33] The reactor model assumes the following statements: (a) plug-flow behavior along the reactor; (b) radial concentration gradients are negligible; (c) axial heat dispersion does not occur; and (d) isothermal behavior is attained. Under these assumptions, the mass balance equation for each lump (Tg, LC, HC, MC, and OC) is written as

$$u_L A\frac{\partial C_i^L}{\partial z} = v_i r_i + \frac{k_i^L a_s A_C}{R_u T_G}(x_i P_i^* - P_i^G) \tag{37}$$

The mathematical model includes a series of equations to consider evaporation for ideal mixing, following the general form for each lump:

$$u_G A\frac{\partial P_i^G}{\partial z} = -\frac{k_i^L a_s A_C}{R_u T_G}(x_i P_i^* - P_i^G) \tag{38}$$

Therefore, the hydrogen evaporation equation is expressed as

$$\frac{\partial P_{H_2}^G}{\partial z} = -\frac{k_{H_2}^L a_s A_C R_u T_G}{U_G}\left(\frac{P_{H_2}^G}{H_{H_2}} - C_{H_2}^L\right) \tag{39}$$

The energy balance was developed to evaluate temperature variations in the catalytic bed for both liquid and gas phases as follows:

Liquid phase:

$$F_G C_p^L\frac{\partial T_L}{\partial z} = \sum r_i \Delta H_i A_C - h_G a_s A(T_G - T_L) - 2\pi r_{in}\varepsilon h_L(T_W - T_L) \tag{40}$$

Gas phase:

$$F_G C_p^G\frac{\partial T_G}{\partial z} = h_G a_s A(T_G - T_L) - 2\pi r_{in}(1-\varepsilon)h_L(T_W - T_G) \tag{41}$$

Considering the configuration of the reactor as a vertical cylinder, the energy balance for the reactor tube is obtained as

$$\lambda_{ax}\frac{\partial^2 T_W}{\partial z^2} + \lambda_{ra}\frac{1}{r}\frac{\partial}{\partial r}\left(\frac{\partial T_W}{\partial r}\right) = 0 \tag{42}$$

To solve these equations, the following boundary conditions were used:

$$r = r_{out} \qquad -k\frac{\partial T}{\partial r} = h_{out}(T - T_{amb}) \tag{43}$$

$$r = r_{in} \qquad -k\frac{\partial T}{\partial r} = h_{in}(T - T_f) \tag{44}$$

$$z = 0 \quad \text{and} \quad z = L \qquad \frac{\partial T}{\partial r} = 0 \tag{45}$$

Liquid, gas, and reactor wall temperature profiles are shown in Figure 7a. The liquid temperature profile increases at the reactor inlet, whereas, in the gas phase, which is fed at the reactor bottom (counter-current flow), temperature increases linearly through the bed, because the physical properties of the gas remain constant under this temperature range. The authors reported that the main product was diesel (Figure 7b). In addition, the model fitted the experimental data well.

Forghani et al.[58] developed a mathematical model of a commercial microscale trickle-bed reactor for oleic acid hydroconversion considering that it is one of the main species present in bio-oil on Ni/β-zeolite as a catalyst. The model involves the concentration of the oleic acid and three specific hydrocarbons (C_9, C_{10}, and C_{12}), which are the major components of jet fuel. Mass transfer between different phases (gas–liquid and liquid–solid) is described by the two-film theory. The reaction rate coefficient, assuming a first-order power-law model for the conversion of oleic acid to middle compounds, was stated as

$$r_{OA} = -k_{OA}C_{OA} \tag{46}$$

$$r_{MC} = k_{MC}C_{OA} \tag{47}$$

DOI: 10.1021/acs.energyfuels.8b00947
Energy Fuels 2018, 32, 7245–7261

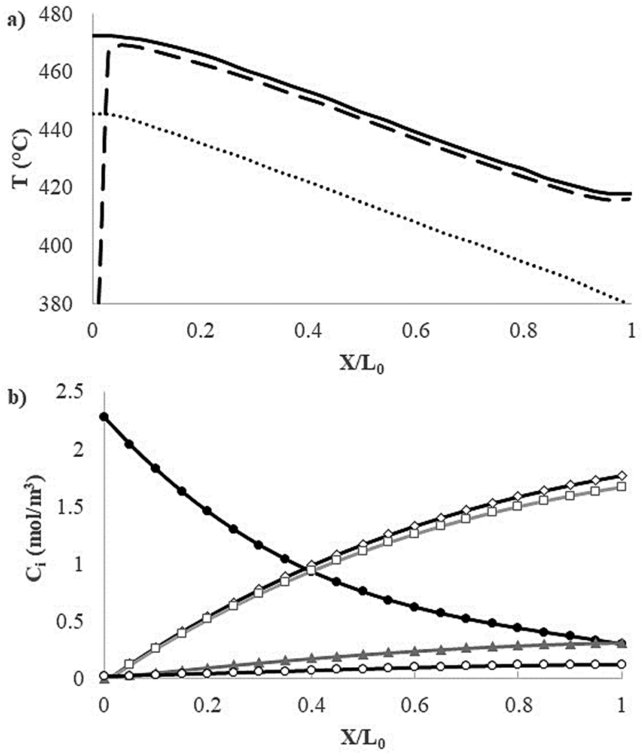

Figure 7. (a) Predicted temperature profiles: solid line (—), wall; dashed line (---), liquid; and dotted line (···), gas. (b) Predicted concentration profiles of triglycerides in a hydrocracking reactor: (●) Tg, (◇) HC, (□) OC, (▲) MC, and (○) LC. Data taken from ref 58.

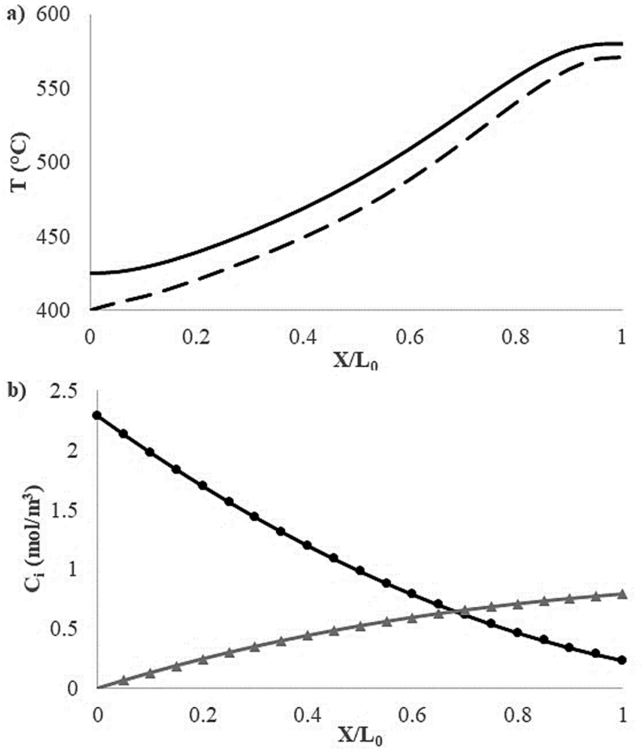

Figure 8. (a) Predicted temperature profiles: solid line (—), wall; and dashed line (– – –), liquid. (b) Predicted concentration profiles of oleic acid in a hydroconversion reactor: (●) OA and (▲) MC. Data taken from ref 57.

The reactor model taking into account the mass balance for oleic acid and middle compounds is

$$u_L A\frac{\partial C_{OA}^L}{\partial z} = -r_{OA} + \frac{k_{OA}^G a_s A_C}{R_u T_g}(x_{OA}P_{OA}^* - P_{OA}^G) \quad (48)$$

$$u_L A\frac{\partial C_{MC}^L}{\partial z} = r + \frac{k_{MC}^L a_s A_C}{R_u T_G}(x_{MC}P_{MC}^* - P_{MC}^G) \quad (49)$$

The energy balance equation for the catalytic bed is represented as

$$F_G C_p^L\frac{\partial T_L}{\partial z} = \sum r_i \Delta H_i A_C - h_G a_s A(T_G - T_L) - 2\pi r_{in}\varepsilon h_L(T_W - T_L) \quad (50)$$

The reactor tube energy balance is represented by eqs 40 and 41.

This equation set was discretized and solved by applying the Gauss−Seidel iteration technique. The liquid and reactor wall temperature profiles increase along the reactor, as shown in Figure 8 and differences among them are due to their heat-transfer coefficients.

The maximum deviation between calculated and experimental data obtained with this model was 7.13% (see Figure 8b). The formation rate of middle compounds decreased throughout the reactor, because the concentration of oleic acid decreases.

Table 6 presents some advantages and disadvantages of the reactor models reported in the literature. Practically, the modeling of vegetable oil hydrotreating reactors is a new field of study and it is necessary to consider some terms in new reactor models or include them into existing ones in order to accomplish the reactor scaling-up at commercial levels. For example, it is mandatory to add terms for mass-transfer limitations, as well as the influence of catalyst particle. Furthermore, nonisothermal or adiabatic operation must be considered.

5. ESTIMATION OF MODEL PARAMETERS

To solve the set of ordinary differential equations (ODEs) and/or partial differential equations (PDEs) that shape the mathematical models, it is necessary to estimate parameters and properties that influence on the system. A series of correlations has been reported to calculate physical and chemical parameters that interact in this process, where the degree of accuracy is of great importance for the mathematical models to converge with experimental data. Table 7 presents a summary of the literature with correlations used to calculate different parameters used during the hydrotreatment of vegetable oil.

Saturation pressure in the liquid/gas interface considered in the mass balance equations along the catalytic bed can be determined by either Henry's law constant or equations of state. Henry's law involves knowledge of the solubility of gaseous components on the liquid phase and the effect of temperature on the process.[51,59] The Henry constant is calculated considering the solubility of compound i (λ_i) and molar volume (v_N) under normal conditions:

$$H_i = \frac{v_N}{\lambda_i \rho_L} \quad (51)$$

On the other hand, because of the novelty of these processes, data of the solubility of hydrogen with vegetable oil compounds are scarce. Therefore, equations of state such as Peng−Robinson or Soave−Redlich−Kwong are used, which have been shown to

DOI: 10.1021/acs.energyfuels.8b00947
Energy Fuels 2018, 32, 7245−7261

Table 6. Comparison of Reactor Models Reported in the Literature

reference of reactor model	advantages	disadvantages
Velez[36]	• It considers the pressure drop of reactor	• The kinetic model underestimated the hydrocarbon concentration particularly at middle conditions
	• It considers the effect of reactor diameter, e.g., reducing the reactor diameter the heat transfer is improved	• The model could be improved considering mass and energy transfer effects
	• It showed that increasing temperature could decrease significantly the catalyst amount	• The model is not validated
	• The energy balance shows that addition of hydrogen for quenching prevents the generation of hot spots	
Boldrini et al.[49]	• It considers the effect of mass transfer resistance in gas/liquid and liquid/solid interfaces, as well as diffusional resistance inside the particle	• It considers only hydrogenation reactions of vegetable oil
	• It considers a catalytic deactivation function and total effectiveness factor reporting a decrease in the activity parameter	
	• The results agree with experimental information showing the increase in conversion of unsaturated compounds by increasing the temperature and catalyst amount	
Forghani et al.[58]	• It considers temperature gradients, as well as temperature effects in reactor tube	• The mass balance shows inconsistencies in dimensional analysis
	• It takes into account evaporation or mass transfer between the gas/liquid interface, showing the decrease in molar fraction distribution and partial pressure of different lumps along the reactor	

Table 7. Correlations Used To Estimate Model Parameters

parameter	ref	parameter	ref
density of liquid phase	61, 62	binary interaction parameter	63−65
dynamic viscosity	61, 62	specific heat capacity	66, 67
gas−liquid mass transfer coefficient	68, 69	enthalpy of vaporization	61
gas−solid mas transfer coefficient	70	Chilton-Colburn factor	71
liquid−solid mas transfer coefficient	72, 73	thermal conductivity	61
gas−liquid interface area	69, 74, 75	thermal conductivity radial	76, 77
gas−solid interface area	78	thermal conductivity axial	79
diffusion coefficient of phase gas	80	pressure drop	81−83

fit well during the hydrotreatment of hydrocarbons reactor modeling:

$$H_i = \lim_{x_i \to 0} \frac{f_{i,\mathrm{L}}}{x_i} = \lim_{x_i \to 0} P\phi_{i,\mathrm{L}} \tag{52}$$

$$P = \frac{RT_\mathrm{f}}{v_\mathrm{f} - b} - \frac{a}{(v_\mathrm{f} + \delta_1 b)(v_\mathrm{f} + \delta_2 b)} \tag{53}$$

where $\phi_{i,\mathrm{L}}$ is the fugacity coefficient of gaseous compounds i in the liquid phase, which is expressed as follows:

$$\ln \phi_{i,\mathrm{L}} = \frac{b_i}{b}(Z_\mathrm{L} - 1) - \ln(Z_\mathrm{L} - B) - \frac{A}{B(\delta_2 - \delta_1)} \left(\frac{2\sum_{k=i}^{N_\mathrm{CL}} x_k a_{ik}}{a} - \frac{b_i}{b} \right) \ln\left(\frac{Z_\mathrm{L} - \delta_2 B}{Z_\mathrm{L} - \delta_1 B} \right) \tag{54}$$

where

$$A = 0.457236\left(\frac{aP}{R_\mathrm{u} T_\mathrm{L}} \right) \tag{55}$$

$$B = 0.077796\left(\frac{bP}{R_\mathrm{u} T_\mathrm{L}} \right) \tag{56}$$

$$A_Z {Z_\mathrm{L}}^3 + B_Z {Z_\mathrm{L}}^2 + C_Z Z_\mathrm{L} + D_Z Z_\mathrm{L} \tag{57}$$

The a and b parameters for a compound mixture are calculated by classical mixing rules:

$$a = a_m = \sum_{i=1}^{N_\mathrm{CL}} \sum_{k=1}^{N_\mathrm{CL}} x_i x_k a_{ij} \tag{58}$$

$$a_{ij} = a_{ji} = \sqrt{a_{ii} a_{jj}}(1 - k_{ij}) \tag{59}$$

$$b = b_m = \sum_{i=1}^{N_\mathrm{CL}} x_i b_i \tag{60}$$

The binary interaction parameter is represented as k_{ij}, and a_{ij} and b_i are the interaction parameters among the different mixture compounds considered by

$$a_i = a_{ii} = a_{c,i}\alpha_i(T) \tag{61}$$

$$a_{c,i} = \frac{{R_\mathrm{u}}^2 {T_{\mathrm{c},i}}^2}{P_{\mathrm{c},i}} \tag{62}$$

$$b_i = \frac{R_\mathrm{u} T_{\mathrm{c},i}}{P_{\mathrm{c},i}} \tag{63}$$

$$\alpha_i(T) = \left[1 + m_i\left(1 - \sqrt{\frac{T_\mathrm{f}}{T_{\mathrm{c},i}}} \right) \right]^2 \tag{64}$$

where m_i is a function of the acentric factor:

$$m_i = M_0 + M_1\omega_i + M_2{\omega_i}^2 \tag{65}$$

The universal parameters (δ_1, δ_2, M_0, M_1, M_2, A_Z, B_Z, C_Z and D_Z) used for the determination of the Henry constant, by means of the state equation, are indicated in Table 8.

The Chilton−Colburn analogy is frequently used to evaluate the heat-transfer coefficients in the gas−liquid and liquid−solid interfaces, considering that $j_\mathrm{H} = j_\mathrm{D}$, because of the lack of correlations to calculate these coefficients. Both coefficients are respectively calculated using the following expressions:

DOI: 10.1021/acs.energyfuels.8b00947
Energy Fuels 2018, 32, 7245−7261

Table 8. Parameters in the Peng–Robinson Equations of State

parameter	value
δ_1	$1 + \sqrt{2}$
δ_2	$1-2$
M_0	0.37464
M_1	1.54226
M_2	−0.26992
A_Z	1
B_Z	$-(1 - B)$
C_Z	$A - 2B - 3B^2$
D_Z	$-(AB - B^2 - B^3)$

$$j_H = \frac{Sh}{Re_f Sc^{1/3}} \quad (66)$$

$$j_D = \frac{Nu}{Re_f Pr^{1/3}} \quad (67)$$

6. CONCLUDING REMARKS

Different types of catalysts, as well as operating conditions and feedstock for the hydrotreatment of vegetable oils has led to the generation of a series of kinetic models. The complexity of such models is dependent on the problem to solve and experimental data available to predict the reaction product distribution. However, in some cases, the power-law models are the preferred ones as the kinetic model. If effects of inhibition of reactive species or products, competition for active sites in catalyst, or adsorption are required, the models such as Langmuir–Hinshelwood and Eley–Rideal have been used.

Among the parameters involved in the models, it was found that temperature and reaction time enhance the conversion of reactive species and increase the hydrogen pressure to promote hydrogenation reaction rate by inhibiting the aromatic compounds and alkenes. Moreover, higher concentration of reactive species increases catalytic deactivation since DCx reactions impact more on catalytic activity than HDO reactions. It is important to consider that reaction rate coefficients are dependent on the alkyl chains length and hydrogen consumption, because of unsaturation of fatty acids. Catalyst activation is an important step for generating data when developing kinetic studies. In most of the reported studies, a reduction process on catalysts based on transition or noble metals has been carried out, which has an affinity for DCx reactions. On the other hand, studies with sulfide catalysts are more dependent on the type of catalytic sites formed on active metals and promoters.

In the kinetic modeling of real feeds, the dependence of kinetic parameters on the properties of feedstock is important and an exaggerated simplification of the system can increase errors when calculating the properties of the reaction system.

Thermal behavior of reactors and even catalyst deactivation are also estimated by mathematical modeling, as a function of the feedstock properties. Catalytic deactivation studies are scarce and, in the case of batch reactors, it is difficult to disclose the effects of chemical reactions and deactivation phenomena occurring during the experimentation.[60]

Based on the developed models, it is observed that, during the reactor modeling for the production of biofuels, mass and heat transfer between phases, pressure drop, and temperature control must be considered, especially in highly exothermic reactions that are more prone to form hot spots. Since renewable fuels produced by hydrotreating is relatively new, deactivation and reactor modeling studies are still necessary to properly design the reactor in order to improve the synthesis of fuels to optimize and predict the yield of fractions from bio-oils accurately.

AUTHOR INFORMATION

Corresponding Author

*E-mail: jancheyt@imp.mx.

ORCID

Jorge Ancheyta: 0000-0001-9626-637X

Notes

The authors declare no competing financial interest.

ACKNOWLEDGMENTS

Authors thank the Mexican Institute of Petroleum for supporting this research project. A.T. also thanks Consejo Nacional de Ciencia y Tecnología (CONACYT) for the Ph.D. scholarship grant.

NOMENCLATURE

Parameters

a_s = specific surface area of catalyst ($m^2\ m^{-3}$)
a_{GL} = gas–liquid mass transfer area per reactor volume (m^{-1})
a_m = geometrical surface area of monolith (m^2)
A_0 = pre-exponential factor (units depending on the type of kinetic)
A = reactor cross section (m^2)
C_i = concentration of species i (mol m^{-3})
$C_{H_2,S}$ = concentration of H_2 at the catalyst surface (mol m^{-3})
$C_{L,i}$ = molar concentration of component i in liquid phase (mol m^{-3})
$C_{G,i}$ = molar concentration of component i in gas phase (mol m^{-3})
C_p = specific heat capacity ($J\ kg^{-1}\ K^{-1}$)
d_p = diameter of particle (m)
d_R = diameter of reactor (m)
D = diffusivity ($m^2\ s^{-1}$)
D_e = effective diffusivity ($m^2\ s^{-1}$)
D_H = hydraulic diameter (m)
E_a = activity energy ($kJ\ mol^{-1}$)
f = fugacity (MPa)
f = fluid
F_G = gas mass flow rate ($kg\ s^{-1}$)
G = gas flux ($kg\ m^{-2}\ s^{-1}$) = Gas phase
h = heat-transfer coefficient ($J\ s^{-1}\ m^{-2}\ K^{-1}$)
H = Henry constant ($Pa\ m^3\ mol^{-1}$)
j_D = Chilton–Colburn j-factor for mass transfer (dimensionless)
j_H = Chilton–Colburn j-factor for energy transfer (dimensionless)
k = reaction rate coefficient (units depending on the type of kinetics)
k' = apparent reaction coefficient ($m^3\ min^{-1}$)
k_{eq} = equilibrium constant
k_d = catalytic decay coefficient (s^{-1})
k_L = mass-transfer coefficient in liquid film ($m\ s^{-1}$)
k_{LS} = liquid–solid mass-transfer coefficient ($m\ s^{-1}$)
k_G = mass-transfer coefficient in gas film ($m\ s^{-1}$)
K_i = adsorption equilibrium coefficient of on catalyst active sites ($m^3\ mol^{-1}$)

DOI: 10.1021/acs.energyfuels.8b00947
Energy Fuels 2018, 32, 7245–7261

K_1' = modified thermodynamic phase equilibrium ratio
$\bar{m}_i$ = molar flow of specie i (mole s^{-1})
n_i = number of moles of species i (mol)
$N_{GL,i}$ = mass transfer flux between gas−liquid film for component i (mol m^{-2} s^{-1})
L = reactor long (m)
L = liquid phase
P = pressure (units depending on the type of system)
P^* = saturation pressure in the liquid−gas phase interface
r = specific reaction rate (units depending on the model type)
R = chemical reaction rate (units depending on the model type)
R_u = constant of ideal gas (units depending on the equation)
t = time (units depending on the type of kinetics)
T = temperature (K)
T_a = thermal fluid temperature (K)
T_B = bulk fluid temperature (K)
T_s = temperature at catalyst surface (K)
u_G = gas velocity (m s^{-1})
u_L = liquid velocity (m s^{-1})
U = overall heat-transfer coefficient (W m^2 K^{-1})
v = stoichiometric coefficient (dimensionless)
v_N = specific molar volume (cm^3 mol^{-1})
V_0 = total volumetric flow (m^3 s^{-1})
V_R = reactor volume (m^3)
W = catalyst weight (kg)
W = Wall
x_i = liquid mole fraction (dimensionless)
Z = compressibility factor (dimensionless)

Greek Symbols

α = function activity (dimensionless)
β = multiplying parameter related to batch deactivation (dimensionless)
γ = temperature-depend parameter (m^3 mol^{-1})
ΔH = differential of heat of reaction (J mol^{-1})
ΔT = differential of temperature (K)
ε = bed porosity (dimensionless)
ϕ_i = fugacity coefficient of gaseous compounds i (dimensionless)
η = overall effectiveness factor (dimensionless)
λ_i = solubility coefficient of component i (Nl i kg^{-1} MPa^{-1})
λ_{ax} = axial thermal conductivity (m^2 s^{-1})
λ_e = effective thermal conductivity of solid (J m^{-1} s^{-1} K^{-1})
λ_{ra} = radial thermal conductivity (m^2 s^{-1})
μ = viscosity (kg m^{-1} s^{-1})
ρ_b = catalyst bulk density (kg m^{-3})
ρ_L = liquid phase density (kg m^{-3})
φ = function describing deactivation phenomenon (dimensionless)
ω = acentric factor (dimensionless)

Subscripts

amb = ambient
c = critical condition
f = fugacity (MPa)
f = fluid
G = gas flux (kg m^{-2} s^{-1})
G = gas phase
H_2 = hydrogen
i = species or component i
in = inside
j = reaction step j
L = reactor long (m) = Liquid phase
out = outside
ref = condition at a reference time
W = catalyst weight (kg)
W = Wall

Superscripts

0 = initial condition of operation
m = reaction order of the gas phase
n = reaction order of the liquid phase

Dimensionless Groups

Nu = Nusselt number
Pr = Prandtl number
Re = Reynolds number
Sc = Schmidt number
Sh = Sherwood number

Abbreviations

DC_x = Decarboxylation/decarbonylation
DDO = direct deoxygenation reaction
FAME = fatty acid methyl esters
FATs = fatty acid triglycerides
HDAL = hexadecanal
HDOL = hexadecanol
HDO = hydrodeoxygenation
HDT = hydrotreatment
HPD = heptadecane
HXD = hexadecane
HYD = hydrogenation reaction
MTS = mesoporous titanosilicate supported
OA = oleic acid
OD = octadecane
ODAL = octadecanal
ODOL = octadecanol
PA = palmitic acid
PD = pentadecane
RBDPO = refined, bleached, and deodorized palm oil
SA = stearic acid
Tg = triglycerides
TBR = trickled-bed reactor
TOFA = tall oil fatty acids
TP = tripalmitin
TS = tristearin

REFERENCES

(1) Arun, N.; Sharma, R. V.; Dalai, A. K. *Renewable Sustainable Energy Rev.* **2015**, *48*, 240−255.
(2) Hermida, L.; Abdullah, A. Z.; Mohamed, A. R. *Renewable Sustainable Energy Rev.* **2015**, *42*, 1223−1233.
(3) Sotelo-Boyas, R.; Liu, Y.; Minowa, T. *Ind. Eng. Chem. Res.* **2011**, *50*, 2791−2799.
(4) He, Z.; Wang, X. *Catal. Sustain. Energy* **2013**, *1* (1), 28−52.
(5) Zhu, X.; Lobban, L. L.; Mallinson, R. G.; Resasco, D. E. *J. Catal.* **2011**, *281*, 21−29.
(6) Saidi, M.; Samimi, F.; Karimipourfard, D.; Nimmanwudipong, T.; Gates, B. C.; Rahimpour, M. R. *Energy Environ. Sci.* **2014**, *7*, 103−129.
(7) Bezergianni, S.; Dimitriadis, A. *Renewable Sustainable Energy Rev.* **2013**, *21*, 110−116.
(8) Boda, L.; Onyestyák, G.; Solt, H.; Lónyi, F.; Valyon, J.; Thernesz, A. *Appl. Catal., A* **2010**, *374* (1−2), 158−169.
(9) Kubička, D.; Kaluža, L. *Appl. Catal., A* **2010**, *372* (2), 199−208.
(10) Chen, N.; Gong, S.; Shirai, H.; Watanabe, T.; Qian, E. W. *Appl. Catal., A* **2013**, *466*, 105−115.
(11) Snåre, M.; Kubičková, I.; Mäki-Arvela, P.; Eränen, K.; Murzin, D. Y. *Ind. Eng. Chem. Res.* **2006**, *45* (16), 5708−5715.

DOI: 10.1021/acs.energyfuels.8b00947
Energy Fuels 2018, 32, 7245−7261

(12) Kubička, D.; Šimáček, P.; Žilkova, N. *Top. Catal.* **2009**, *52* (1−2), 161−168.
(13) Furimsky, E. *Catal. Today* **2013**, *217*, 13−56.
(14) Mortensen, P. M.; Grunwaldt, J.; Jensen, P. A.; Knudsen, K. G.; Jensen, A. D. *Appl. Catal., A* **2011**, *407* (1−2), 1−19.
(15) Hermida, L.; Abdullah, A. Z.; Mohamed, A. R. *Renewable Sustainable Energy Rev.* **2015**, *42*, 1223−1233.
(16) Snåre, M.; Kubičková, I.; Mäki-Arvela, P.; Eränen, K.; Wärnå, J.; Murzin, D. Y. *Chem. Eng. J.* **2007**, *134* (1−3), 29−34.
(17) Kumar, P.; Yenumala, S. R.; Maity, S. K.; Shee, D. *Appl. Catal., A* **2014**, *471*, 28−38.
(18) Ayodele, O. B.; Farouk, H. U.; Mohammed, J.; Uemura, Y.; Daud, W. M. A. W. *J. Taiwan Inst. Chem. Eng.* **2015**, *50*, 142−152.
(19) Zhang, H.; Lin, H.; Wang, W.; Zheng, Y.; Hu, P. *Appl. Catal., B* **2014**, *150−151*, 238−348.
(20) Bie, Y.; Kanervo, J. M.; Lehtonen, J. *Ind. Eng. Chem. Res.* **2015**, *54* (48), 11986−11996.
(21) Bie, Y.; Lehtonen, J.; Kanervo, J. *Appl. Catal., A* **2016**, *526*, 183−190.
(22) Yenumala, S. R.; Maity, S. K.; Shee, D. *React. Kinet., Mech. Catal.* **2017**, *120* (1), 109−128.
(23) Zhang, H.; Lin, H.; Zheng, Y. *Appl. Catal., B* **2014**, *160−161* (1), 415−422.
(24) Gevert, B. S.; Eriksson, M.; Eriksson, P.; Massoth, F. E. *Appl. Catal., A* **1994**, *117*, 151−162.
(25) Jeništová, K.; Hachemi, I.; Mäki-Arvela, P.; Kumar, N.; Peurla, M.; Čapek, L.; Wärnå, J.; Murzin, D. Y. *Chem. Eng. J.* **2017**, *316*, 401−409.
(26) Hachemi, I.; Murzin, D. Y. *Chem. Eng. J.* **2018**, *334*, 2201−2207.
(27) Grilc, M.; Likozar, B.; Levec, J. *Biomass Bioenergy* **2014**, *63*, 300−312.
(28) Grilc, M.; Likozar, B.; Levec, J. *Appl. Catal., B* **2014**, *150−151*, 275−287.
(29) Fernández, M. B.; Tonetto, G. M.; Crapiste, G.; Damiani, D. E. *Int. J. Chem. React. Eng.* **2007**, *5*, Article A10 (DOI: 10.2202/1542-6580.1380).
(30) Zhang, S.; Yan, Y.; Li, T.; Ren, Z. *Energy Sources, Part A* **2009**, *31* (8), 639−645.
(31) Selishcheva, S. A.; Lebedev, M. Y.; Reshetnikov, S. I.; Trusov, L. I.; Yakovlev, V. A. *Catal. Ind.* **2014**, *6* (1), 60−66.
(32) Sharma, R. K.; Anand, M.; Rana, B. S.; Kumar, R.; Farooqui, S. A.; Sibi, M. G.; Sinha, A. K. *Catal. Today* **2012**, *198* (1), 314−320.
(33) Anand, M.; Sinha, A. K. *Bioresour. Technol.* **2012**, *126*, 148−155.
(34) Sinha, A. K.; Anand, M.; Rana, B. S.; Kumar, R.; Farooqui, S. A.; Sibi, M. G.; Kumar, R.; Joshi, R. K. *Catal. Surv. Asia* **2013**, *17* (1), 1−13.
(35) Anand, M.; Farooqui, S. A.; Kumar, R.; Joshi, R.; Kumar, R.; Sibi, M. G.; Singh, H.; Sinha, A. K. *Appl. Catal., A* **2016**, *516*, 144−152.
(36) Vélez Manco, J. F. Conceptual design of a palm oil hydrotreatment reactor for commercial diesel production. M.S. Thesis, Universidad Nacional de Colombia, Sede Medellín Facultad de Minas, Medellín, Colombia, 2014.
(37) Sheu, Y. H. E.; Anthony, R. G.; Soltes, E. J. *Fuel Process. Technol.* **1988**, *19* (1), 31−50.
(38) Zhang, S.-P. *Energy Sources* **2003**, *25* (1), 57−65.
(39) Zhou, L.; Lawal, A. *Appl. Catal., A* **2017**, *532*, 40−49.
(40) Sebos, I.; Matsoukas, A.; Apostolopoulos, V.; Papayannakos, N. *Fuel* **2009**, *88* (1), 145−149.
(41) Vonortas, A.; Kubička, D.; Papayannakos, N. *Fuel* **2014**, *116*, 49−55.
(42) Alcázar, L. A.; Ancheyta, J. *Chem. Eng. J.* **2007**, *128* (2−3), 85−93.
(43) Laurent, E.; Delmon, B. *Ind. Eng. Chem. Res.* **1993**, *32* (11), 2516−2524.
(44) Şenol, O. I.; Ryymin, E. M.; Viljava, T. R.; Krause, A. O. I. J. *Mol. Catal. A: Chem.* **2007**, *277* (1−2), 107−112.
(45) Romero, Y.; Richard, F.; Brunet, S. *Appl. Catal., B* **2010**, *98* (3−4), 213−223.
(46) Lauritsen, J. V.; Bollinger, M. V.; Lægsgaard, E.; Jacobsen, K. W.; Nørskov, J. K.; Clausen, B. S.; Topsøe, H.; Besenbacher, F. *J. Catal.* **2004**, *221*, 510−522.
(47) Chianelli, R. R. *Catal. Rev.: Sci. Eng.* **1984**, *26*, 361−393.
(48) Li, K.; Wang, R.; Chen, J. *Energy Fuels* **2011**, *25*, 854−863.
(49) Boldrini, D. E.; Damiani, D. E.; Tonetto, G. M. *AIChE J.* **2014**, *60* (10), 3524−3533.
(50) Edvardsson, J.; Rautanen, P.; Littorin, A.; Larsson, M. *J. Am. Oil Chem. Soc.* **2001**, *78* (3), 319−327.
(51) Mederos, F. S.; Elizalde, I.; Ancheyta, J. *Catal. Rev.: Sci. Eng.* **2009**, *51* (4), 485−607.
(52) Cabrera, M. I.; Grau, R. J. *Int. J. Chem. React. Eng.* **2008**, *6*, 1−37.
(53) Takeya, K.; Konishi, H.; Kawanari, M.; Chiba, T.; Sanada, Y. *Food Sci. Technol. Int., Tokyo* **1997**, *3* (1), 10−16.
(54) Fillion, B.; Morsi, B. I.; Heier, K. R.; Machado, R. M. *Ind. Eng. Chem. Res.* **2002**, *41* (4), 697−709.
(55) Holser, R. A.; List, G. R.; King, J. W.; Holliday, R. L.; Neff, W. E. *J. Agric. Food Chem.* **2002**, *50* (24), 7111−7113.
(56) Chen, A. H.; Mclntire, D. D.; Allen, R. R. *J. Am. Oil Chem. Soc.* **1981**, *58* (8), 816−818.
(57) Forghani, A. A.; Lewis, D. M. *J. Chem. Technol. Biotechnol.* **2016**, *91* (3), 655−663.
(58) Forghani, A. A.; Jafarian, M.; Pendleton, P.; Lewis, D. M. *Int. J. Energy Res.* **2014**, *38*, 1624−1634.
(59) Geana, D.; Steiner, R. *J. Supercrit. Fluids* **1995**, *8* (2), 107−118.
(60) Perego, C.; Peratello, S. *Catal. Today* **1999**, *52*, 133−145.
(61) Yaws, C. L. *Thermophysical Properties of Chemicals and Hydrocarbons*; William Andrew: Norwich, NY, 2009.
(62) Cruz-Forero, D. C.; González-Ruiz, O. A.; López-Giraldo, L. J. *CT&F-Cienc., Tecnol. Futuro* **2012**, *5*, 67−82.
(63) Moysan, J. M.; Huron, M. J.; Paradowski, H.; Vidal, J. *Chem. Eng. Sci.* **1983**, *38* (7), 1085−1092.
(64) Nishiumi, H.; Arai, T.; Takeuchi, K. *Fluid Phase Equilib.* **1988**, *42*, 43−62.
(65) Gao, G.; Daridon, J. L.; Saint-Guirons, H.; Xans, P.; Montel, F. *Fluid Phase Equilib.* **1992**, *74* (C), 85−93.
(66) Morad, N. A.; Kamal, A. A. M.; Panau, F.; Yew, T. W. *J. Am. Oil Chem. Soc.* **2000**, *77* (9), 1001−1005.
(67) Cedeño, F. O.; Prieto, M. M.; Xiberta, J. *J. Chem. Eng. Data* **2000**, *45* (1), 64−69.
(68) Goto, S.; Smith, J. M. *AIChE J.* **1975**, *21* (4), 706−713.
(69) Al-dahhan, M. H.; Larachi, F.; Dudukovic, M. P.; Laurent, A. *Ind. Eng. Chem. Res.* **1997**, *36*, 3292−3314.
(70) Dwivedi, P. N.; Upadhyay, S. N. *Ind. Eng. Chem. Process Des. Dev.* **1977**, *16* (2), 157−165.
(71) Chilton, T. H.; Colburn, A. P. *Ind. Eng. Chem.* **1934**, *26*, 1183−1187.
(72) Duduković, M. P.; Larachi, F.; Mills, P. L. *Catal. Rev.: Sci. Eng.* **2002**, *44* (1), 123−246.
(73) Speccia, V.; Baldi, G.; Gianetto, A. *Ind. Eng. Chem. Process Des. Dev.* **1978**, *17* (3), 362−367.
(74) Venkata Ratnam, G. S.; Venkata Narasaiah, D.; Varma, Y. B. G. *Bioprocess Eng.* **1994**, *10*, 53−59.
(75) Venkata Ratnam, G. S.; Varma, Y. B. G. *Bioprocess Eng.* **1991**, *7*, 29−34.
(76) Chu, C. F.; Ng, K. M. *Chem. Eng. Commun.* **1985**, *37* (1−6), 127−140.
(77) Bey, O.; Eigenberger, G. *Int. J. Therm. Sci.* **2001**, *40*, 152−164.
(78) Puranik, S. S.; Vogelpohl, A. *Chem. Eng. Sci.* **1974**, *29* (2), 501−507.
(79) Dixon, A. G. *AIChE J.* **1985**, *31* (5), 826−834.
(80) Fuller, E. N.; Schettler, P. D.; Giddings, J. C. *Ind. Eng. Chem.* **1966**, *58*, 18−27.
(81) Al-Dahhan, M. H.; Khadilkar, M. R.; Wu, Y.; Duduković, M. P. *Ind. Eng. Chem. Res.* **1998**, *37* (3), 793−798.
(82) Çarpinlioğlu, M. Ö.; Özahi, E. *Powder Technol.* **2008**, *187* (1), 94−101.
(83) Larkins, R. P.; White, R. R.; Jeffrey, D. W. *AIChE J.* **1961**, *7* (2), 231−239.

DOI: 10.1021/acs.energyfuels.8b00947
Energy Fuels 2018, 32, 7245−7261